Agricultural and Forest Meteorology 372 (2025) 110709

Contents lists available at ScienceDirect

Agricultural and Forest Meteorology

journal homepage: www.elsevier.com/locate/agrformet

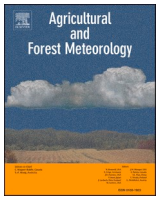

Predicting maize production in Northeastern China: Unraveling the influence of summer compound heat-drought events through physical mechanisms

Yeran Zhou [a], Huixin Li [a,b,c,*], Bo Sun [a,b,c], Huijun Wang [a,b,c], Hui Ju [d,e], Yuan Yuan [a], Jiani Zeng [a]

[a] State Key Laboratory of Climate System Prediction and Risk Management/Key Laboratory of Meteorological Disaster, Ministry of Education/Collaborative Innovation Center on Forecast and Evaluation of Meteorological Disasters, Nanjing University of Information Science and Technology, Nanjing, China
[b] Southern Marine Science and Engineering Guangdong Laboratory, Zhuhai, China
[c] Nansen-Zhu International Research Centre, Institute of Atmospheric Physics, Chinese Academy of Sciences, Beijing, China
[d] Institute of Environment and Sustainable Development in Agriculture, Chinese Academy of Agricultural Sciences, Beijing, China
[e] Key Laboratory of Agricultural Environment, Ministry of Agriculture and Rural Affaire of PR China, Beijing, China

ARTICLE INFO

Keywords:
Northeastern China
Maize production
Compound heat-drought events
Atmospheric circulation
Prediction models

ABSTRACT

Northeastern China (NEC), known as the granary of China, is significantly affected by compound heat-drought events (CHDEs), which have detrimental impacts on maize production. This study aims to investigate the physical mechanisms underlying the occurrences of CHDEs on maize production in NEC. Our findings indicate that CHDEs are associated with anomalous positive geopotential height at 500 hPa, the presence of anticyclone at 850 hPa and a uniform downward motion in NEC, all of which are adverse to maize production. Using a year-to-year increment method, we reveal that several key factors collectively influence CHDEs and maize production in NEC, including sea ice concentration in the Barents Sea in May, sea surface temperature (SST) in the equatorial East Pacific in February and March, soil water over northwestern Siberia in April, and the North Atlantic Oscillation (NAO) in February. To differentiate the diverse influences of these key factors on CHDEs and maize production, we developed two distinct prediction models (Prediction Model #1 and #2). Both Prediction Model #1 ($r = 0.90$, $p < 0.01$) and #2 ($r = 0.91$, $p < 0.01$) demonstrate high correlation coefficients between predicted and observed values, as validated through leave-one-out cross-validation (Prediction Model #1: $r = 0.90$, $p < 0.01$; Prediction Model #2: $r = 0.90$, $p < 0.01$) and independent hindcasts (Prediction Model #1: $r = 0.72$, $p < 0.01$; Prediction Model #2: $r = 0.79$, $p < 0.01$). This study provides precise predictions of maize production in eastern China, offering significant safeguards for national food security.

1. Introduction

Maize is one of China's primary food crops, serving as a cash crop, feed source, and industrial raw material (Erenstein et al., 2022). Northeastern China (NEC) accounts for approximately 30 % of the nation's total maize production (Kent et al., 2019), highlighting its importance in national agricultural output. However, agriculture in this region is highly vulnerable to climate change (Ha et al., 2021), facing substantial risks from extreme weather events such as heatwaves and droughts, which can severely damage crops (You et al., 2009; Lesk et al., 2016; Zhang and Hu., 2018; Song et al., 2020, 2021; Wang et al., 2020). The detrimental impact is particularly pronounced during compound heatwaves and droughts events (Li et al., 2018; Lesk et al., 2021). For instance, the severe drought events in summer 2014 caused crop damage across China amounting to 5 million hectares, with 2.95 million hectares were affected in NEC (https://europe.chinadaily.com.cn/china/2014–08/21/content_18462617.htm). Additionally, the high-temperature drought event in 2018 (Zeng et al., 2019) led to a 30 % reduction in soybean and maize production in NEC, leading to significant economic losses (https://www.cma.gov.cn/en/). Estimates suggest that a 1 °C increase in temperature can lead to a 10 % decrease in food production (Song et al., 2021). Furthermore, the frequency and severity of droughts associated with heatwaves in NEC have surged in recent decades (Chen and Sun., 2015), which is expected to further impact

* Corresponding author at: Nanjing University of Information Science & Technology, No.219, Ningliu Road, Nanjing, Jiangsu, China (Postcode: 210044).
E-mail address: lihuixin@nuist.edu.cn (H. Li).

https://doi.org/10.1016/j.agrformet.2025.110709
Received 27 December 2024; Received in revised form 18 June 2025; Accepted 23 June 2025
Available online 3 July 2025

maize production.

Maize thrives in warm and humid conditions, with temperature playing a crucial role throughout its growth stages (Lesk et al., 2016, 2021; Wu et al., 2024). In NEC, sufficient thermal conditions during the maize growing season prolong the growth period, mitigate cold stress (Ju et al., 2013), augment photosynthetic activity, and consequently lead to an increase in maize production. However, the ongoing trend of global warming, which has led to increasingly extreme heat events, poses a considerable threat to maize production (Tao et al., 2012; Webber et al., 2018; Li et al., 2022b). The high temperature stress during the growth cycle exert a profound impact on maize production, particularly during the flowering and filling stages, which are highly susceptible to high temperatures (Li et al., 2022a). Specifically, exposure to high temperatures during flowering and filling stages affects pollination (Wang et al., 2019b; Liu et al., 2020), accelerates leaf senescence, reduces photosynthetic rates (Kim et al., 2023), disrupts carbohydrate metabolism and starch biosynthesis (Liu et al., 2022), ultimately influencing kernel number and weight in maize (Liu et al., 2022). Furthermore, these temperature-sensitive growth stages of maize coincide with the summer season in NEC, during which heat events are increasingly prevalent (Li et al., 2018, 2023), causing the peak temperatures typically experienced by maize to align with the sensitive stage (Tao et al., 2016; Ma et al., 2020). With the occurrence of summer heatwaves, the temperature-moisture coupling effect exacerbated by high temperatures further intensify the heat sensitivity of maize (Lesk et al., 2021), thereby adversely affecting maize growth.

Drought is also a primary factor inhibiting maize growth (Aroca et al., 2003; Lesk et al., 2016, 2021; Kim et al., 2023), with previous studies indicating that drought events can result in a reduction of 25–30 % in maize production (Campos et al., 2004). Severe drought conditions lead to soil moisture deficits that fail to meet the water requirements of crops during their critical growth stages (Chatterjee et al., 2022). The increasing potential evaporation and the decreasing soil moisture heighten the demand for agricultural irrigation, exacerbating water supply-demand conflicts (Ju et al., 2013). Furthermore, drought events are projected to become more frequent and intense, leading to curling of maize leaves, which inhibits photosynthesis and impedes maize growth (Bai et al., 2006; Nielsen et al., 2009; Kim et al., 2023). These changes amplify the adverse effects on maize production and pose significant challenges to regional food security (Haro-Monteagudo et al., 2017; Webber et al., 2018). In recent years, significant yield reductions of major food crops globally due to drought have been reported (Venkatappa et al., 2021), underscoring the substantial impact of drought on agricultural productivity. Therefore, the occurrence of compound heat-drought events (CHDEs) in NEC are poised to substantially diminish maize production in the region.

Recent studies have highlighted the associations between CHDEs in NEC and several influential factors. He et al. (2018) noted that the presence of sea ice in Barents Sea in June could influence summer precipitation in East Asia through Silk Road and Pacific-Japan teleconnections. Additionally, Tian et al. (2021) suggested that Bering Sea ice during the melting season affects summer precipitation in Northeastern Asia through its interaction with North Atlantic Sea temperature. Chen and Sun. (2024) explored the impacts of Arctic Sea ice on temperature and crop production in China, while Li et al. (2022a) identified potential mechanisms through which Barents Sea ice, sea surface temperature (SST) and soil moisture interact to influence CHDEs in NEC during July and August. These findings underscore the role of sea ice (Wang et al., 2019a; Tian et al., 2021; Chen et al., 2022; Chen and Sun., 2024), especially in Barents Sea (He et al., 2018; Li et al., 2018, 2022a; Lin et al., 2018; Du et al., 2021), in affecting temperature and precipitation in China by influencing teleconnection patterns, such as the Polar-Eurasian (POL) teleconnection (Chen et al., 2022; Li et al., 2022a). Additionally, a La Niña-Like SST condition in February can affect the Pacific-Japan teleconnection wave train through air-sea interactions (Wen et al., 2022), subsequently impacting climate conditions in NEC. Sun et al. (2021) further explored the consequences of increased snowmelt in Eastern Europe and Western Siberia during spring, noting its effect on land surface warming in Northeast Asia during summer. Jiang et al. (2023) examined the extreme high temperature experienced in eastern China during the summer of 2022, elucidating the role of North Atlantic triple SST (NAT) in fostering anticyclonic circulation anomalies over eastern China through mid-latitude Rossby wave trains.

In addition to atmospheric circulation mechanisms, recent studies have underscored the role of temperature-moisture couplings in amplifying CHDEs. Ni et al. (2024) found that during the 2022 CHDEs in the Yangtze River Basin, low soil moisture shifted a larger proportion of surface net radiation toward sensible heat rather than latent heat, exacerbating heat and drought conditions via land-atmosphere positive feedback. Similarly, Seo et al. (2022) showed that CHDEs in Northeast Asia are closely tied to local land-atmosphere interactions.

Interannual climate variability explains about 60 per cent of the maize production variability globally (Ray et al., 2015). Previous studies have established prediction models for maize production in NEC based on various climate variability predictors. For instance, Zhou et al. (2013) demonstrated that the North Atlantic Oscillation (NAO) can trigger a Rossby wave response in the upper troposphere of Eurasia via the generation of NAT anomalies in spring. This atmospheric anomaly pattern subsequently influences air temperature in NEC, thereby affecting maize production. Zhou and Wang (2014) further illustrated that Bering Sea ice enhances the subtropical high pressure over the western Pacific, which leads to positive precipitation anomalies in NEC. The greenhouse effect of water vapor from these precipitation anomalies raises minimum temperature, promoting maize growth. Consequently, Zhou et al. (2017) developed a maize production prediction model specific to NEC, incorporating NAO and Bering Sea ice as key predictors. Additionally, Chen and Sun (2024) devised a nonlinear regression prediction model that elucidates the direct and indirect impacts of Arctic Sea ice on temperature and crop production in China.

Despite these advancements, previous researches have primarily focused on the thermal conditions necessary for maize, neglecting a comprehensive look at the impacts of CHDEs on maize production. However, in the context of accelerating global warming, it is anticipated that high-temperature stress will increasingly influence maize production (Lesk et al., 2016), highlighting the necessity for prediction models that integrate CHDEs. Moreover, existing maize production prediction models for NEC have predominantly centered on sea ice and NAO, often overlooking other climatic variabilities that indirectly influence maize production through CHDEs.

This study aims to address the following questions: What are the physical mechanisms through which antecedent meteorological factors influence maize production via CHDEs in NEC during the summer? How can we develop a more accurate prediction model with extended validity periods for maize production in this region? The structure of this paper is as follows: Section 2 details the datasets and methodologies employed in this study. Section 3 presents the primary findings, including the relationship between maize production and meteorological factors in NEC, the potential physical mechanisms by which four internal climatic variabilities affect maize production amidst CHDEs, and the establishment, validation, and comparison of two prediction models for maize production in NEC. Finally, Section 4 concludes with a summary of the key findings.

2. Data and methods

2.1. Study area

This study focuses on NEC, a region critical for maize production. Geographically, NEC encompasses Heilongjiang province, Jilin province, Liaoning province, and five cities in the eastern Inner Mongolia Autonomous Region. Notably, Heilongjiang province, Jilin province and Liaoning province account for a significant portion of the total maize

production in NEC, contributing approximately 75 % during 1979–2020 (https://data.stats.gov.cn/english/), whereas the contribution from Inner Mongolia Autonomous Region is comparatively smaller. Previous research has shown that 73 % of Inner Mongolia Autonomous Region's maize production is concentrated in its eastern part (Yu et al., 2023), which aligns closely with the five cities in the eastern Inner Mongolia Autonomous Region mentioned earlier. Given this distribution, the average maize production from Heilongjiang province, Jilin province, Liaoning province and Inner Mongolia Autonomous Region serves as a suitable representation of maize production within NEC. Accordingly, we have defined the study area based on the regional boundaries of NEC and the distribution of maize production, as illustrated by the green rectangle (110°E–135°E, 41°N–54°N) in Fig. 1a.

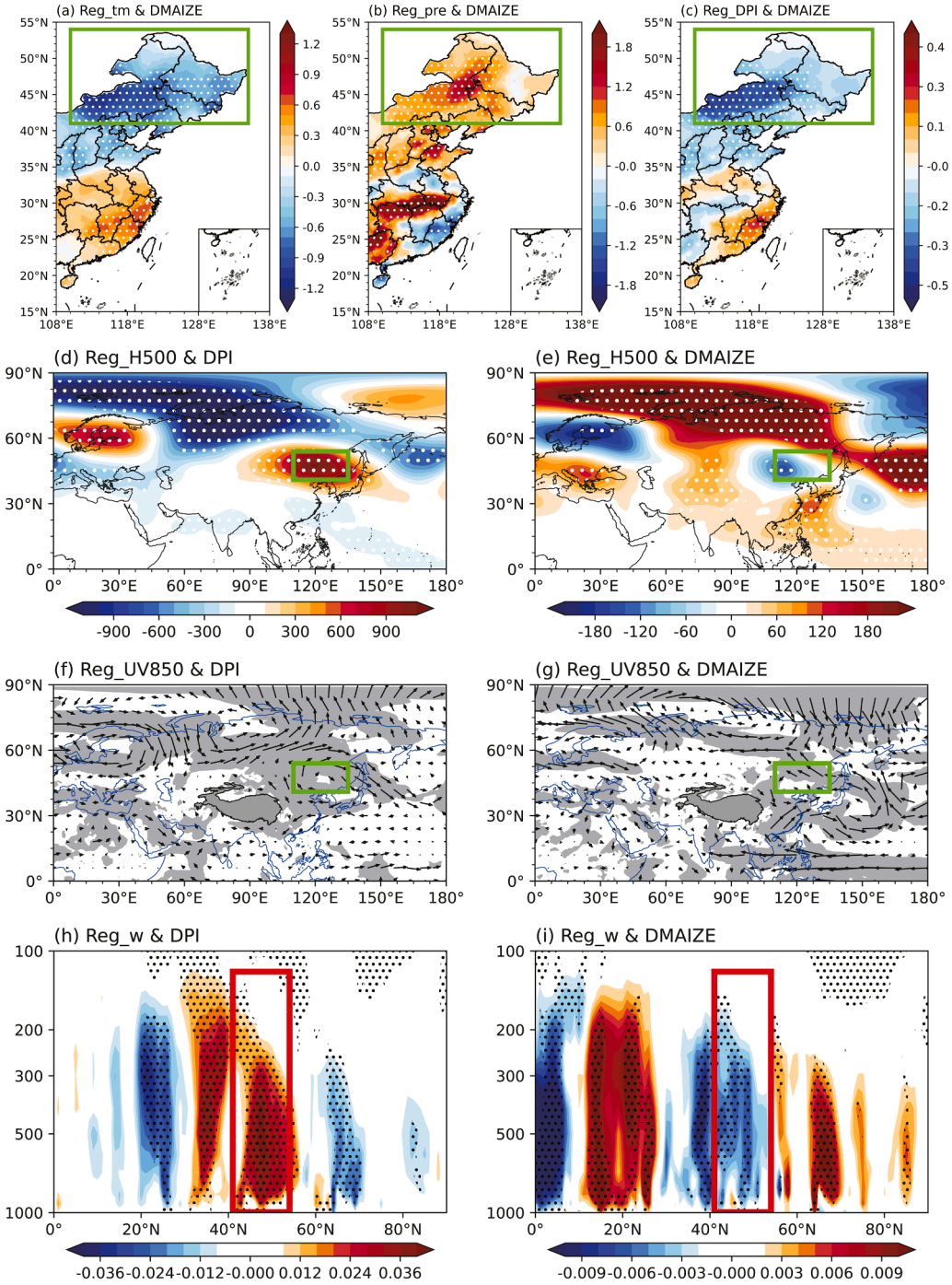

Fig. 1. Regression maps of the summer (a) temperature, (b) precipitation and (c) DPI with regard to DMAIZE during 1980–2020. Regression maps of the anomalous atmospheric circulations in summer with regard to DPI during 1980–2020: (d) 500 hPa geopotential height, (f) 850 hPa wind, (h) vertical velocity averaged along 110°E–135°E vertical-latitudinal cross section. Regression maps of the anomalous atmospheric circulations in summer with regard to DMAIZE: (e) 500 hPa geopotential height, (g) 850 hPa wind, (i) vertical velocity averaged along 110°E–135°E vertical-latitudinal cross section. The regression coefficients within the dotted (gray-shade) areas are statistically significant at the 90 % confidence level based on the Student's *t*-test. The green rectangles denote NEC, whereas the red rectangle signifies the airspace over NEC.

2.2. Data

2.2.1. Data sources

Monthly gridded temperature and precipitation data during 1979–2020 are sourced from the CN05.1 datasets at 0.25° × 0.25° resolution. The CN05.1 data (Wu and Gao, 2013) is constructed based on over 2000 ground-based meteorological observation station data from the China Meteorological Administration, which is a continuously updated data. The ERA5 reanalysis dataset (https://cds.climate.copernicus.eu/), developed by the European Centre for Medium-Range Weather Forecasts, provides monthly meteorological reanalysis datasets for this study. Specifically, the following variables are utilized: geopotential height, zonal and meridional winds, vertical velocity, relative humidity, specific humidity, fraction of cloud cover, mean surface net short wave radiation flux, mean surface sensible heat flux, 2-m temperature, sea level pressure, volumetric soil water layer 1 and sea surface temperature, with a spatial resolution of 1° × 1°. Monthly sea ice concentration data are obtained from the Hadley Center, with a spatial resolution of 1° × 1°. Maize production data are sourced from the National Bureau of Statistics of China (https://data.stats.gov.cn/english/), which are the annual provincial per unit area maize production data.

Regarding data utilization: The gridded temperature and precipitation data from CN05.1 are employed for two primary purposes: the calculation of the CHDEs Index (PI) and the illustration of relationships between large-scale climate factors and temperature, precipitation, as well as CHDEs conditions in NEC. The monthly gridded reanalysis data from ERA5, including geopotential height, zonal and meridional winds, vertical velocity, relative humidity, fraction of cloud cover, mean surface net short wave radiation flux, mean surface sensible heat flux and 2-m temperature, are utilized to investigate the atmospheric circulation patterns in NEC and key regions of large-scale climate factors through regression analysis. Additionally, the geopotential height, zonal, and meridional wind data are used to compute wave activity flux, while the specific humidity, zonal, and meridional wind data are employed to calculate water vapor flux. Moreover, the sea level pressure, volumetric soil water layer 1 and sea surface temperature data from ERA5, along with sea ice concentration data from the Hadley Center, are used to examine the relationships between CHDEs and large-scale climate factors, as well as to define key factor indices. Furthermore, the maize production per unit area data from the National Bureau of Statistics are utilized to compute the maize production index.

2.2.2. Data preprocessing

The year-to-year increment method is utilized to mitigate the impact of non-meteorological factors on maize production in NEC. Prior researches have demonstrated the year-to-year increment method's efficacy in de-trending data (Dai et al., 2021), and the continuous economic growth coupled with advancements in maize varieties has led to a notable upward trend in maize production over recent decades, diminishing signals of interannual variability in maize production. To isolate the influence of climatic variables on maize production from non-meteorological factors and enhance interannual variability signals in maize production, the year-to-year increment approach is employed, which is calculated as the difference between the current year's and the preceding year's values (Fan et al., 2008). For instance, $DMAIZE(2025) = MAIZE(2025) - MAIZE(2024)$.

Furthermore, meteorological variables also exhibit pronounced long-term trends that may obscure the signals of interannual variability. These trends can potentially compromise the accuracy of the study findings by overshadowing the subtle patterns of interannual fluctuations. To better characterize the interannual variability of meteorological factors, all meteorological data have been comprehensively processed using the year-to-year increment methods in this study, effectively isolating the interannual variability component and removing the long-term trends. It is noteworthy that the original data cover the period from 1979 to 2020. However, due to the unique computational requirements of the year-to-year increment method, the time range of the processed data is adjusted to 1980–2020 in this study.

The standardization process, denoted as Z, involves adjusting the data such that the mean approaches zero and the standard deviation approaches one. The formula for this calculation is provided as: $z = \frac{x-\mu}{\sigma}$, x denotes the raw data, μ signifies the mean of the data, and σ indicates the standard deviation of the data. In this study, maize production and climate factors exhibit different dimensionalities. Despite having conducted year-to-year increment methods previously, dimensional discrepancies persist between maize production and climate factors. When constructing a regression model with climate factors as independent variables to predict maize production, the regression coefficients lack comparability due to the differing scales of variables, which may also lead to model bias (Bring, 1994). Therefore, prior to constructing the prediction models, all factors underwent a standardization process to unify their dimensionalities and scales, among which the standardized year-to-year increment regional mean of PI index in NEC during summer months (June, July and August) is designated as DPI, whereas the standardized year-to-year increment maize production is referred to as DMAIZE.

2.3. Statistical analysis

2.3.1. Quantifying CHDEs

The index PI, which characterizes the severity of CHDEs, is introduced in this study to assess the impact of summer CHDEs on maize production quantitatively. The establishment of PI relies on joint survival cumulative distribution of temperature and precipitation in NEC. Firstly, the cumulative distribution are denoted as $F_1(x_1) = P(X_1 \le x_1)$(precipitation) and $F_2(x_2) = P(X_2 \le x_2)$ (temperature), which are used to calculate the individual return period of precipitation deficit and high temperature events ($R_i(x_i) = \frac{1}{1-F_i(x_i)}$). Next, by using t-copula method and the survival cumulative distribution of precipitation and temperature ($\overline{F_i} = 1 - F_i$), the joint survival cumulative distribution functions (CDF) of precipitation deficit and high temperature events are defined as:

$$PI = C[\overline{F_1}(x_1), \overline{F_2}(x_2)] = P(X_1 > x_1, X_2 > x_2) \quad (1)$$

It is noteworthy that a lower value of PI indicates a more severe CHDEs (Li et al., 2018, 2020, 2022a). Therefore, the PI values are multiplied by (− 1) to enhance comprehension in this study, such that a higher PI index signifies more severe CHDEs.

2.3.2. Identifying key factors affecting CHDEs

Previous studies have identified that Arctic sea ice (He et al., 2018; Li et al., 2018, 2022a, 2025; Lin et al., 2018; Wang et al., 2019a; Du et al., 2021; Tian et al., 2021; Chen et al., 2022; Chen and Sun., 2024), sea surface temperature (Li et al., 2022a, 2025; Wen et al., 2022; Jiang et al., 2023; Du et al., 2025), soil moisture (Li et al., 2022a; Sang et al., 2022; Du et al., 2025), and the North Atlantic Oscillation (Zhou et al., 2013, 2017; Zhang et al., 2021; Hao et al., 2022) may influence East Asian temperature and precipitation. Building upon these findings, regression analysis is employed to identify the key factors affecting CHDEs and maize production, which are selected based on their potential influence on NEC climate and agricultural outcomes. The methodology involves two critical steps: (1) statistical significance testing to identify regions where these meteorological factors exhibited strong correlations with both the PI and maize production; (2) physical mechanism validation to refine the identified regions. This two-step process ensure that the selected regions are both statistically significant and physically plausible.

Eventually, the standardized regional mean of sea ice concentration in Barents Sea region (20°E–47°E, 72°N–78°N) in May, soil water in northwestern Siberia (30°E–110°E, 60°N–75°N) in April, which are directly linked to CHDEs and maize production, are denoted as SICI and

SWI respectively. It is noteworthy that the specific months and key regions of SST that exert an influence on CHDEs and maize production differ significantly. Consequently, two SST indices, SSTPI and SSTMI, are defined here to represent the standardized regional mean of SST in equatorial East Pacific (130°W–80°W, 20°S–5°N) in February and in equatorial East Pacific (130°W–80°W, 10°S–15°N) in March, respectively. Additionally, the NAO in February, directly associated with CHDEs and maize production, is defined as NAOI, quantified as:

$$NAOI = Z(SS1 - SS2) \quad (2)$$

where SS1 and SS2 represent the regional mean of sea level pressure for regions S1 (60°W–0°W, 70°N–75°N) and S2 (80°W–0°W, 15°N–36°N), as illustrated in Fig. 6a. The positive phase of NAO occurs when the regional mean sea level pressure in S1 is positive, while that in S2 is negative.

2.4. Statistical modeling and evaluation

To address the issue of covariance in modeling, a stepwise regression method is employed to develop predicting models (Carnes and Slade, 1988) in this study. Partial correlation analysis can examine the independent relationship between two variables while controlling for the influence of other variables (Yule, 1907). It eliminates the interference of other variables to more accurately understand the direct relationship between variables. To further validate the independence of factors during model construction, partial correlation analysis was conducted among all candidate predictors. The relative importance of factors was assessed through standardized regression coefficients Beta (Menard, 2004; Tonidandel and LeBreton, 2021), with the total explained variance determined by summing squared Beta values (Cohen et al., 2003). Contribution rates of individual factors were subsequently calculated by dividing each factor's squared Beta coefficient by the total explained variance, ensuring comparability across variables (Cohen et al., 2003; Darlington et al., 2017).

Additionally, we assess the reliability and validity of the prediction models derived from this method using leave-one-out cross-validation and independent hindcast tests. In leave-one-out cross-validation tests, data from one year is reserved as the test set, while the data from the remaining years are served as the training set (Bishop, 2006; Fan, 2010). For instance, a dataset spanning 41 years during 1979–2020, excluding 1990, can be used to predict data for 1990. The independent hindcast tests utilize data from preceding years to sequentially forecast subsequent years. For instance, a dataset during 1979–2019 can serve as the training set to forecast data for 2020. Given the unique computational requirements of independent hindcast tests, the results for the earlier portion of the time series (years closer to 1979) in this study spanning the period from 1979 to 2020 may lack statistical significance due to insufficient modeling data. Therefore, this study present independent hindcast tests only for the latter portion of the time series in this study, specifically from 1996 to 2020 (Fig. S24 and S26).

3. Results

3.1. Correlation between meteorological factors and maize production in NEC

Fig. 1 demonstrates a significant correlation between maize production and summer mean temperature and precipitation in NEC during 1980–2020. Results indicate a significant negative relationship ($r = -0.33, p < 0.05$) between maize production and temperature (Fig. 1a and S1a) and a significant positive relationship ($r = 0.48, p < 0.01$) between maize production and precipitation (Fig. 1b and S1b) during summer. Additionally, maize production exhibits a negative correlation with DPI (Fig. 1c), indicating that the occurrence of CHDEs may adversely affect maize production. Specifically, maize plants are characterized by their tall stature and broad leaves. Extreme drought conditions during summer can cause the leaves of maize to curl (Kim et al., 2023), reducing the photosynthetic area and efficiency, ultimately adversely impacting maize production. Additionally, extreme hot events shorten the maize growing season, hinder the induction of flowering in male inflorescences, disrupt pollen development (Kim et al., 2023) and intensify the heat sensitivity of maize through temperature-moisture coupling effects (Lesk et al., 2021), thereby exerting a significant adverse influence on maize production. Consequently, the combination of high temperature and water deficits during summer poses a significant threat to maize production (Fig. 1c), particularly in arid and semi-arid regions such as NEC (Ju et al., 2013). Overall, negative anomalies in temperature and positive anomalies in precipitation are crucial for mitigating the impacts of CHDEs in NEC in summer, further substantiating the inverse relationship between maize production and CHDEs in this region.

Heilongjiang province, Jilin province and Liaoning province are situated closer to the coast in NEC, which results in higher annual precipitation and superior water vapor conditions compared to the more inland Inner Mongolia Autonomous Region (Fig. S2). According to the global aridity classification established by the United Nations Environment Programme, which defines the aridity index as the ratio of annual precipitation to potential evapotranspiration (Zomer et al., 2022), the Inner Mongolia Autonomous Region exhibits a higher degree of aridity than the three northeastern provinces (Zomer et al., 2022). This regional disparity in aridity renders Inner Mongolia Autonomous Region more vulnerable to CHDEs. Consequently, agricultural systems in this region, particularly maize during its growing season, are subjected to more severe impacts from these climatic extremes. The statistical relationships between maize production and temperature, precipitation, and PI are more pronounced in Inner Mongolia Autonomous Region (Fig. 1).

The regression analysis of DPI and maize production in relation to atmospheric circulation in NEC during summer are presented in Fig. 1. The findings suggest that the occurrence of CHDEs in this region are associated with specific atmospheric anomalies. Notably, a positive geopotential height center at 500 hPa (Fig. 1d), an anticyclonic wind at 850 hPa (Fig. 1f) and a uniform downward motion (Fig. 1h) over NEC are observed. The significant downward motion associated with the positive geopotential height anomaly over NEC results in a negative anomaly in cloud cover (Fig. S3e). This reduction in cloud blockage enhances surface net short wave radiation (Fig. S3f), subsequently leading to an increase in temperature (Fig. S3a). Additionally, the anomalous anticyclonic circulation at 850 hPa prevents the accumulation of water vapor (Fig. S3c). Combined with the cloudless anomaly, these factors ultimately contribute to a negative anomaly in wet condition (Fig. S3d) and precipitation (Fig. S3b) over NEC.

In contrast, increased maize production coincides with a pronounced negative geopotential height anomaly at 500 hPa (Fig. 1e), a cyclonic anomaly at 850 hPa (Fig. 1g) and a uniform upward motion anomaly (Fig. 1i) over NEC. These atmospheric anomalies promote favorable conditions for increased cloud cover (Fig. S4c), which hinders the increase in surface net short wave radiation (Fig. S4d), resulting in negative temperature anomalies (Fig. 1a). Furthermore, these atmospheric circulations enhance water vapor content (Fig. S4a and S4b), contributing to positive precipitation anomalies (Fig. 1b) in NEC. Therefore, the atmospheric circulation patterns associated with CHDEs are fundamentally in contrast with those related to enhanced maize production. Positive precipitation anomalies and negative temperature anomalies in summer are beneficial for maize growth, ultimately facilitating increased maize production in NEC.

3.2. Physical mechanisms associated with maize production in NEC

3.2.1. Influence of sea ice concentration in the Barents sea

Previous studies have demonstrated that the sea ice in the Barents Sea exerts a significant impact on China's climate (Petoukhov and Semenov, 2010; Inoue et al., 2012; Kim et al., 2014; Lin et al., 2018;

Chen et al., 2022). The sea ice concentration in Barents Sea is strongly correlated with summer CHDEs (Fig. S5) and maize production (Fig. S6), with both correlations peaking in May (Fig. 2a, 2b and S7) and persisting into the following summer (Fig. 2c), similar to the results of Du et al. (2021). Notably, the correlation coefficient between SICI in May and maize production during 1980–2020 is 0.33, which is significant at the 95 % confidence level based on the Student's *t*-test (Fig. S7). In contrast, the correlation coefficient between SICI in May and DPI during 1980–2020 is –0.50, significant at the 99 % confidence level according to the same test (Fig. S7).

Fig. 2 presents regression maps of summer atmospheric circulation with respect to SICI. The results reveal an anomalous upward-downward-upward pattern over the "northwestern Eurasia-polar region-northeastern China" at 200 hPa (Fig. 2i), which exhibit similarities to the Polar/Eurasian (POL) teleconnection pattern. Previous studies have elucidated the possible mechanisms through which springtime Barents Sea ice influences summer CHDEs in NEC (Li et al., 2018, 2022a). On one hand, the growth of sea ice in the Barents Sea in spring results in cooler temperatures, which subsequently lower temperatures across western Eurasia. This cooling phenomenon contributes to an increase in snow depth in the region (Gao et al., 2015; Li et al., 2018; Chen et al., 2022), ultimately enhancing soil moisture levels in May and June in NEC by influencing atmospheric processes (Li et al., 2018). Soil moisture exerts a critical role in drought dynamics by modulating evaporation-precipitation feedbacks and atmosphere-land energy exchanges (Li et al., 2018), with effects that can persist for two to three months (Zhang and Zuo., 2011; Chen et al., 2022). Consequently, soil moisture conditions in May and June in NEC may carry over into the summer months, thereby influencing summer CHDEs (Li et al., 2018). On the other hand, sea ice exhibits significant memory, allowing the increased sea ice concentration signal in May to persist into the summer months in the Barents-Kara Seas (Fig. 2c). The atmospheric disturbances induced by intensified sea ice in summer stimulate upward wave trains reaching 200 hPa in the Barents-Kara Seas (He et al., 2018), which in turn enhances a southeastward-propagating POL teleconnection wave train (Fig. 2i) during summer.

The POL teleconnection wave train further influences atmospheric circulation in NEC in summer. Specifically, the negative geopotential

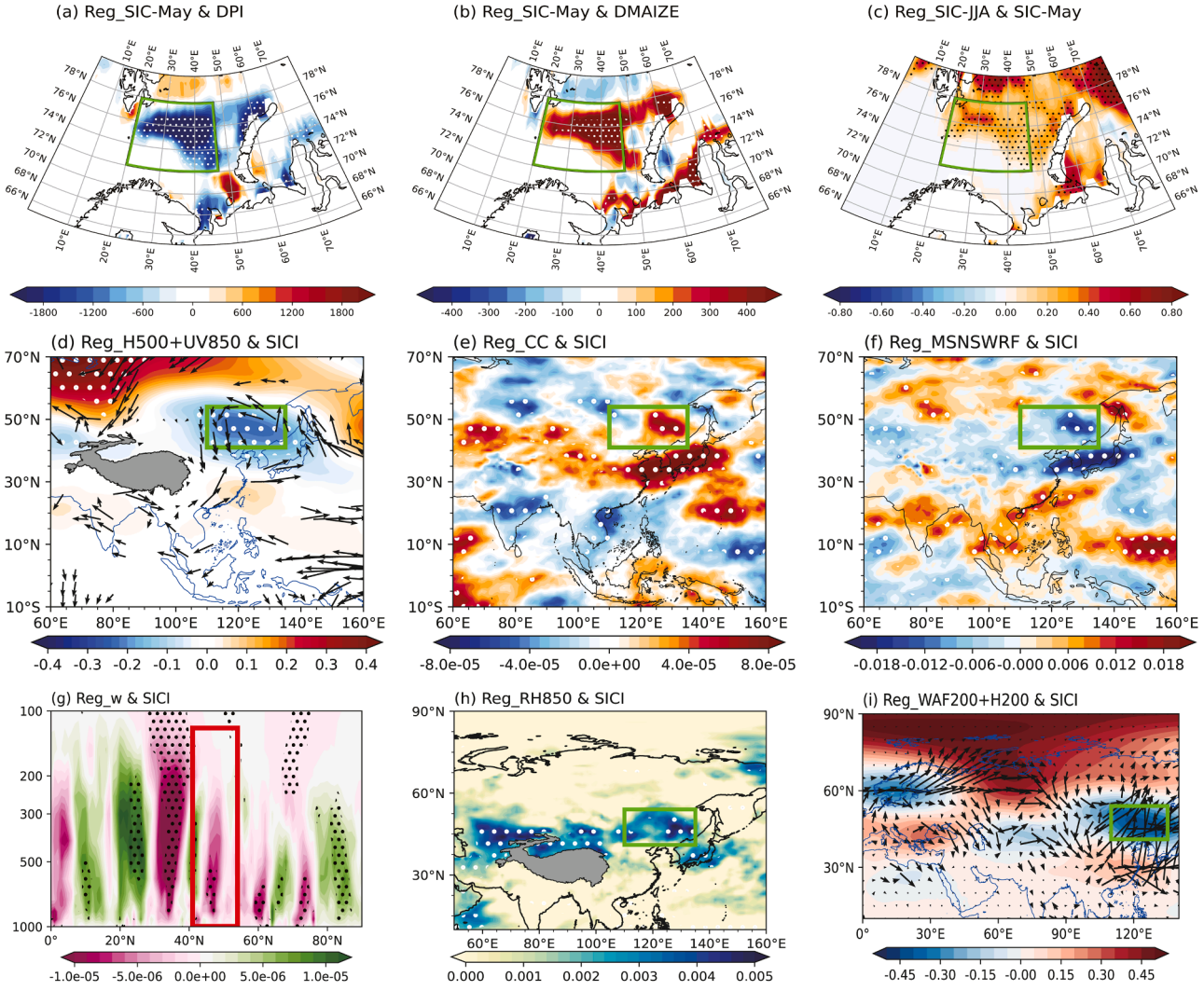

Fig. 2. Regression maps of sea ice concentration in May with regard to (a) DPI, (b) DMAIZE during 1980–2020. Regression maps of (c) sea ice concentration in summer with regard to SICI and the anomalous atmospheric circulations in summer with regard to SICI during 1980–2020: (d) 500 hPa geopotential height (shading) & 850 hPa wind (arrow), (e) fraction of cloud cover, (f) surface net short wave radiation flux, (g) vertical velocity averaged along 110°E–135°E vertical-latitudinal cross section, (h) 850 hPa relative humidity, (i) 200 hPa wave flux (arrow) & geopotential height (shading). The regression coefficients within the dotted areas are significant at the 90 % confidence level based on the Student's *t*-test. The green rectangles in Fig. 2a, 2b and 2c denote the sea ice concentration key regions for this study, where the regional mean of sea ice concentration is defined as SICI in May. The green rectangles in Fig. 2d, 2e, 2f, 2h and 2i denote NEC, whereas the red rectangle in Fig. 2g signifies the airspace over NEC.

height anomaly at 500 hPa (Fig. 2d), coupled with cyclonic wind anomaly at 850 hPa (Fig. 2d) and significant upward motion anomaly from 1000 hPa to 300 hPa (Fig. 2g) over NEC, induce robust convective activity and enhance water vapor transport, ultimately leading to increased cloud cover in the region (Fig. 2e). This enhanced cloud cover contributes to lower temperatures (Fig. S8a) by reducing surface net short wave radiation (Fig. 2f) and promotes precipitation (Fig. S8b) through increased wetness at 850 hPa (Fig. 2h) during summer. Consequently, this atmospheric circulation pattern effectively prevents CHDEs, moderates the detrimental impacts of extreme heat on maize growth duration, and alleviates drought-induced leaf curling in maize, ultimately enhancing maize production in the NEC.

3.2.2. *Influence of El Niño-like SST pattern*

CHDEs exhibit a significant correlation with SST in the equatorial East Pacific during years characterized by the decay of La Niña conditions (Fig. S9). This correlation is associated with an La Niña-like SST pattern observed in the preceding winter, which subsequently diminishes during the summer months (Fig. S9 and S11). In contrast, the relationship between maize production and SST in the equatorial East Pacific approximately reflects an inverse pattern to that of CHDEs. Specifically, the presence of a winter El Niño-like SST pattern in the preceding season, along with a summer La Niña-like SST pattern, exhibits a significant positive correlation with maize production, as illustrated in Fig. S10.

However, the correlations between SST and CHDEs and maize production exhibit notable inconsistencies. Specifically, the peak correlation between SST and CHDEs occurs in February (denoted as SSTPI) (Fig. 3a and S11), similar to the results of Li et al. (2022a), whereas the maximum correlation for maize production is observed in March (denoted as SSTMI) (Fig. 3b and S11). The correlation coefficient between SSTPI and DPI is –0.28, which is significant at the 90 % confidence level according to the Student's *t*-test. In contrast, the correlation coefficient between SSTMI and maize production is 0.46, demonstrating significance at the 99 % confidence level based on the same test.

Both SSTPI and SSTMI exhibit significant correlations with the Nino3.4 SST index (170°W–120°W, 5°S–5°N) during the same period (Fig. S12). However, given the robust and statistically significant relationships between these customized SST indices (SSTPI and SSTMI) and both CHDEs and maize production, SSTPI and SSTMI are utilized to represent the equatorial East Pacific SST in this study, rather than depending solely on the Nino index.

Fig. 3 further presents regression maps that highlight the relationship between SSTPI and atmospheric circulation in summer. Notably, a wave train resembling Pacific-Japan teleconnection pattern at 500 hPa is distinctly observed, characterized by anomalous atmospheric

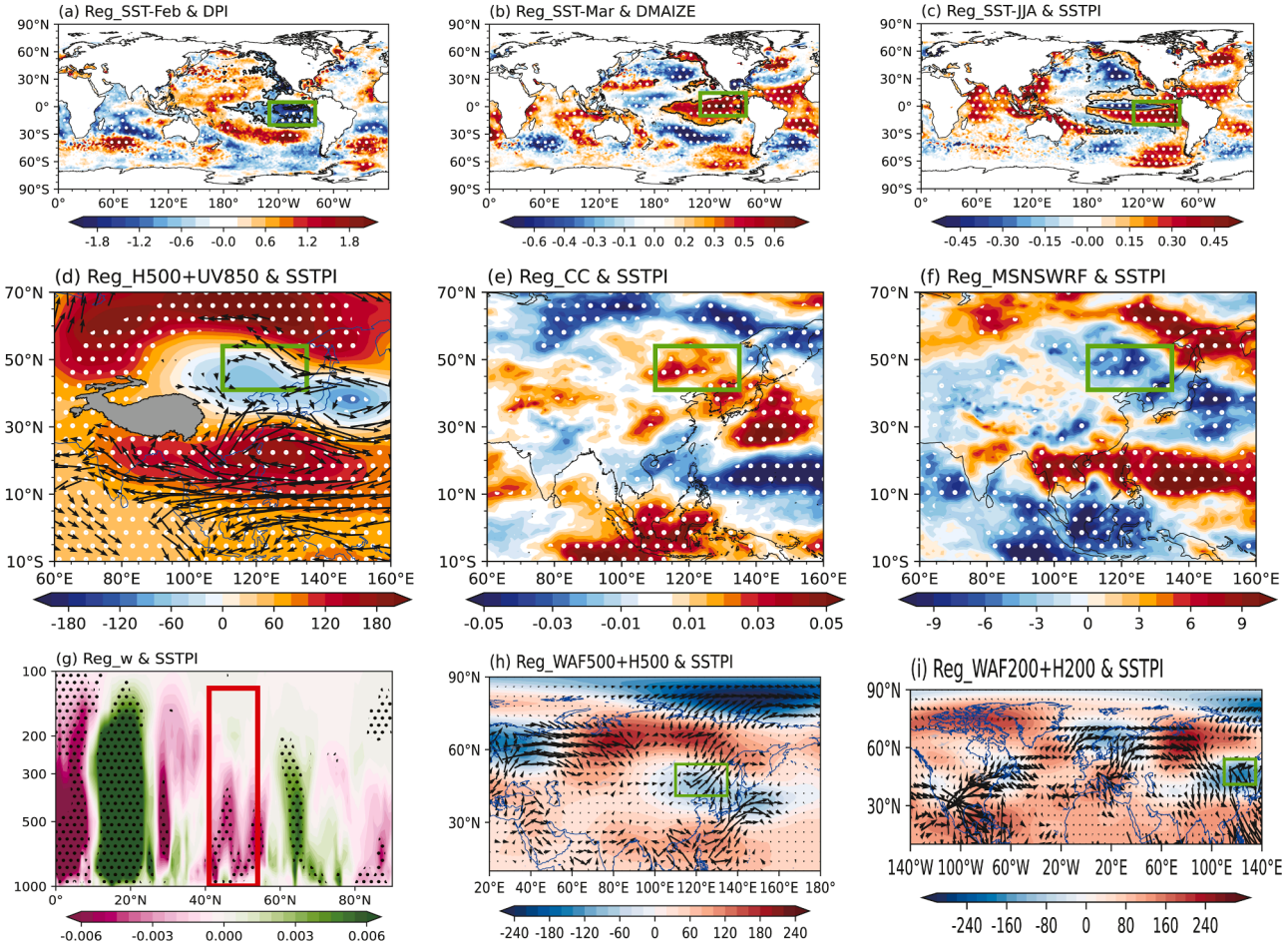

Fig. 3. Regression maps of (a) SST in February with regard to DPI and (b) SST in March with regard to DMAIZE during 1980–2020. Regression maps of (c) SST in summer with regard to SSTPI and the anomalous atmospheric circulations in summer with regard to SSTPI during 1980–2020: (d) 500 hPa geopotential height (shading) & 850 hPa wind (arrow), (e) fraction of cloud cover, (f) surface net short wave radiatioin flux, (g) vertical velocity averaged along 110°E–135°E vertical-latitudinal cross section, (h) 500 hPa wave flux (arrow) & geopotential height (shading), (i) 200 hPa wave flux (arrow) & geopotential height (shading). The regression coefficients within the dotted areas are significant at the 90 % confidence level based on the Student's *t*-test. The green rectangles in Fig. 3a, 3b and 3c denote the SST key regions for this study, where the regional mean of SST is defined as (a) SSTPI in February, (b) SSTMI in March. The green rectangles in Fig. 3d, 3e, 3f, 3h and 3i denote NEC, whereas the red rectangle in Fig. 3g signifies the airspace over NEC.

circulation features indicative of positive-negative geopotential height across the "northwestern Pacific-northeastern China" region (Fig. 3h). Previous studies have established that the positive SST anomalies in the equatorial East Pacific in winter can persist into summer (Fig. S10) via the "capacitor effect" in the Indian Ocean (Fig. 3c) (Xie et al., 2009). Warm SST anomalies in the Indian Ocean exert a significant influence on the warming of the overlying atmospheric temperature through moist-adiabatic adjustment processes (Xie et al., 2009). Furthermore, the enhanced tropospheric temperature over the Indian Ocean drives the formation of eastward-propagating equatorial Kelvin waves (Feng et al., 2021, 2022), which in turn trigger divergence in the subtropics through the Ekman divergence mechanism (Wu et al., 2009, 2010; Xie et al., 2009). The resultant subtropical divergence subsequently leads to suppressed convection (Fig. 3e and 3f) and the formation of an anomalous anticyclone in the northwestern Pacific (Fig. 3d and 3h), which further enhances the intensity of the Western North Pacific Anomalous Anticyclone (Xie et al., 2009; Chen et al., 2017; Zhu et al., 2023). The strengthening of the Western North Pacific Anomalous Anticyclone at 500 hPa further intensifies the Pacific-Japan teleconnection wave train (Fig. 3h), which propagates northwards along the East Asian coast through NEC (Zhu et al., 2023).

Moreover, a notable eastward propagating wave train, extending from the eastern North Pacific to NEC, is evident in the regression of SSTPI against the 200 hPa wave flux (Fig. 3i). CHDEs in NEC exhibit a significant correlation with La Niña-like SST and "Z-shaped" cold SST patterns in the North Pacific during the preceding winter (Fig. 3a). The "Z-shaped" cold SST pattern during winter is characterized by the combined influence of La Niña-like SST anomalies in the equatorial East Pacific and warm SST anomalies in the North Pacific, with narrow cold SST anomalies extending along the west coast of North America and connecting to the main body of La Niña-like SST anomalies (Wen et al., 2022). As summer arrives, the La Niña-like SST anomalies in the equatorial East Pacific weaken and transition to El Niño-like SST anomalies. Cold SST anomalies persist on the northwest and southwest flanks of the El Niño-like SST anomalies and connect at its west side (Wen et al., 2022). Coupled with the narrow cold SST anomalies along the North American coast, the overall SST anomaly pattern exhibits a "Z-shaped" cold SST anomaly structure. In contrast, the correlation between maize production and SST in the preceding winter shows an inverse pattern to that of CHDEs, with El Niño-like SST and "Z-shaped" warm SST patterns observed (Fig. 3b). Previous research has indicated that La Niña-like SST anomalies during the preceding winter can lead to the formation of a "Z-shaped" cold SST pattern in the Northeastern Pacific (Li et al., 2025) from winter to summer (Wen et al., 2022), triggered by poleward Kelvin waves (Chelton et al., 1982; Li et al., 2025). The resulting SST pattern amplifies atmospheric disturbances, which in turn induce the upward and northward-propagating Rossby waves in the tropical Pacific. These perturbations then enter the subtropical westerly jet stream at 200 hPa (Wen et al., 2022), and propagate from the North Pacific towards NEC, contributing to an increase in hot and drought events in NEC (Wen et al., 2022). Therefore, a positive correlation emerges between the El Niño--like SST during the preceding winter and maize production in NEC. The "Z-shaped" warm SST pattern stimulates Rossby wave train from North Pacific to NEC at 200 hPa, contributing to the atmospheric circulation favourable for maize growth in NEC in summer. Consequently, we propose that El Niño-like SST anomalies exert a significant influence on the atmospheric circulation over NEC through two distinct physical mechanisms operating at the 200 hPa and 500 hPa levels, respectively.

Influenced by two wave trains triggered by SST anomalies in the equatorial East Pacific, a pronounced negative geopotential height anomaly at 500 hPa (Fig. 3d), a cyclonic wind anomaly at 850 hPa (Fig. 3d), and an upward motion anomaly from 1000 hPa to 300 hPa (Fig. 3g) are observed over NEC. The enhanced negative geopotential height and upward motion lead to decreased cloud cover over NEC during summer (Fig. 3e), resulting in a negative anomaly in surface net short wave radiation (Fig. 3f). This sequence of events subsequently results in a decrease in temperature (Fig. S13a). Moreover, the significant southeasterly wind on the northwestern flank of the cyclonic circulation anomaly at 850 hPa facilitate the transport a substantial amount of water vapor from the sea to NEC (Fig. 3d), thereby establishing favorable moisture conditions in this region. When combined with the dynamic conditions of convergence, this situation enhances precipitation rates in NEC (Fig. S13b). Consequently, the observed decrease in temperature (Fig. S13a) and the increase in precipitation (Fig. S13b) contribute to slowdown in CHDEs over NEC in summer, which is advantageous for maize production. Additionally, the summer atmospheric circulation regression maps associated with SSTMI exhibit patterns similar to those linked to SSTPI (Fig. S14).

3.2.3. Influence of soil water in northwestern Siberia

Both CHDEs (Fig. S15) and maize production (Fig. S16) exhibit a significant correlation with soil water in northwestern Siberia, with the strongest correlation observed in April (Fig. 4a, 4b and S17), similar to results of Li et al. (2022a). Specifically, the Student's *t*-test indicates that soil water shows a positive correlation ($r = 0.54, p < 0.01$) with DPI and a negative correlation ($r = -0.65, p < 0.01$) with maize production in NEC (Fig. S17).

The regression map of SWI* [$SWI^* = SWI \times (-1)$] for summer 200 hPa wave flux reveals a wave train centered over Siberia and NEC at mid- to high latitudes (Fig. 5f). However, the question arises: how does the soil water in April sustain its influence and subsequently affect the atmospheric circulation during summer? A stationary atmospheric wave train may have been present at 500 hPa over Eurasia in April (Fig. 4d), characterized by "positive-negative-positive" geopotential height anomalies in three regions: northern Europe, Siberia, and northeastern China. The northerly wind anomaly on the western flank of the cyclonic circulation in Siberia facilitates the influx of cold air from the north (Fig. 4d), leading to unusually cold (Fig. 4e) and wet (Fig. 4e) weather conditions during April and May. This reduction in ground evaporation caused by the cold and wet weather impedes the evaporation of soil moisture. Consequently, the suppression of evaporation lessens the evaporation cooling effect, leading to warmer condition in Siberia in June (Fig. 4f). This shift in weather patterns triggers a reversal in atmospheric circulation, characterized by a positive geopotential height anomaly at 500 hPa in northwestern Siberia during the subsequent summer (Fig. 5a). Additionally, the warm atmospheric conditions in June intensify soil evaporation, resulting in negative soil water anomalies in Siberia in summer (Fig. 4c). This indicates that the negative soil water anomalies observed in northwestern Siberia in April can persist into the summer due to ongoing atmospheric processes, similar to results of Li et al. (2022a).

Consequently, the positive geopotential height anomaly at 500 hPa in Siberia during summer, amplified by the negative soil moisture anomaly in April, reinforces the propagation of the wave train (Fig. 5f), which in turn influences the atmospheric circulation conditions over NEC. Specifically, the intensified negative geopotential height anomalies at 500 hPa (Fig. 5a), coupled with cyclonic wind anomalies at 850 hPa (Fig. 5a) and upward motion anomalies from 1000 hPa to 300 hPa (Fig. 5c) in NEC, contribute to increased cloud cover (Fig. 5b) and enhanced water vapor (Fig. 5b and 5e). These changes further lead to reduced temperatures (Fig. S18a) and increased precipitation (Fig. S18b) by impacting surface net shortwave radiation (Fig. 5d) and atmospheric moisture content (Fig. 5e). These anomalous temperature and precipitation conditions are crucial roles for mitigating the impacts of high temperature stress and water deficits on maize production.

3.2.4. Influence of North Atlantic oscillation

In addition to the aforementioned influencing factors, Zhou et al. (2013) have demonstrated a significant relationship between the NAO and maize production in NEC. Specifically, CHDEs (Fig. 6a and S19) and maize production (Fig. 6b and S20) in NEC exhibit a significant NAO-like correlation pattern with the sea level pressure in February. The

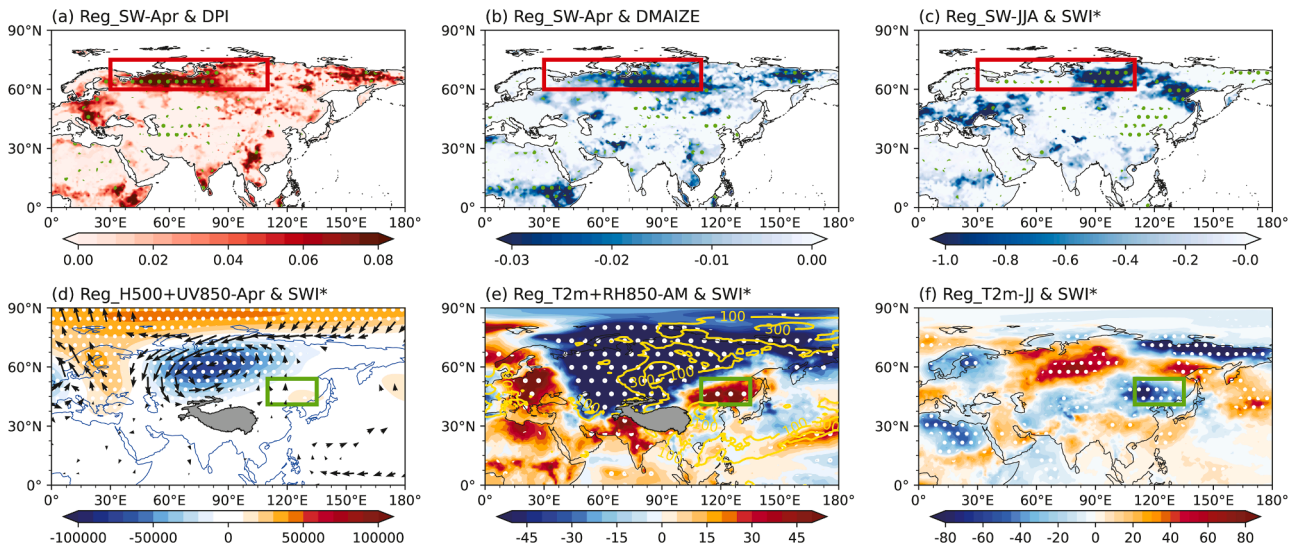

Fig. 4. Regression maps of soil water in April with regard to (a) DPI, (b) DMAIZE during 1980–2020. Regression maps of (c) soil water in summer with regard to SWI* [$SWI^* = SWI \times (-1)$] and the anomalous atmospheric circulations with regard to SWI* during 1980–2020: (d) 500 hPa geopotential height (shading) & 850 hPa wind (arrow) in April, (e) surface 2-m air temperature (shading) & 850 hPa relative humidity (isoline) in April and May, (f) surface 2-m air temperature in June and July. The regression coefficients within the dotted areas are significant at the 90 % confidence level based on the Student's *t*-test. The red rectangles denote the soil water key regions for this study, where the regional mean of soil water in April is defined as SWI. The green rectangles denote NEC, the study area in this study.

correlation coefficient between NAOI and DPI is –0.31, which is significant at the 95 % confidence level. Furthermore, the correlation coefficient between NAOI and maize production is 0.44, significant at the 99 % confidence level (Fig. S21).

NAOI regression maps of wave flux and geopotential height at 200 hPa in summer reveal a prominent wave train extending from the North Atlantic to NEC, as well as a wave train enhancing in the polar region (Fig. 7f). Both of these wave patterns exert a non-negligible influence on the climatic conditions in NEC. However, the correlation between NAO and both maize production and DPI exhibited considerable variability in the months following February, with most months failing to demonstrate statistically significant correlations (Fig. S21). Given the transient nature of atmospheric signals, this raises an intriguing question regarding the persistence of NAO signal from February into summer, and how it subsequently influence CHDEs in NEC. Consequently, we further explore the intermediate roles of NAT and Arctic Sea ice.

Previous studies have highlighted the significant interaction between NAO and NAT systems, illustrating that the NAO signal can be perpetuated through the influence of the triple SST (Fig. 6d and S22). This persistence is facilitated by intense air-sea interaction (Cui et al., 2015; Zhang et al., 2021; Hao et al., 2022). The NAT pattern persists into the summer (Fig. 6d), driven by positive feedback mechanisms between the NAO and NAT, as well as the memory characteristics of SST. Consequently, the NAT enhances the atmospheric disturbance through increased baroclinicity, which stimulates an eastward-propagating wave train extending from the North Atlantic to NEC (Fig. 7f) in summer, significantly impacting atmospheric circulation over NEC (Zhou et al., 2017).

Moreover, NAO exerts a notable influence on temperature and precipitation in East Asia, mediated by the "capacitor" effect of Arctic Sea ice during spring (Zhang et al., 2021). NAO signal in February can last into the spring (Fig. 6c). Regression analyses of NAOI on the surface 2-m air temperature and 850 hPa wind in spring reveal that an intensification of NAOI correlates with northeasterly wind in the Barents Sea. These anomalies transport cold air from polar regions, resulting in decreased temperature in this area (Fig. 6e). Concurrently, sufficient water vapor transport at 850 hPa (Fig. 6f) enhances the spring sea ice concentration in the Barents Sea (Fig. 6f), which subsequently influences atmospheric circulation in NEC through the POL wave train.

The aforementioned wave trains give rise to a negative geopotential height anomaly at 500 hPa (Fig. 7a), a cyclonic wind anomaly at 850 hPa (Fig. 7a), and a significant upward motion anomaly from 1000 hPa to 300 hPa (Fig. 7c) over NEC. These anomalies are associated with increased cloud cover (Fig. 7b), which in turn reduces surface net shortwave radiation (Fig. 7d), ultimately contributing to a decrease in temperature over NEC (Fig. S23a). Additionally, the pronounced cyclonic circulation anomaly in NEC promotes southeasterly winds that transport substantial amounts of water vapor into the region (Fig. 7a and 7b), leading to unusually wet conditions in NEC (Fig. 7e). In summary, the interplay of these dynamical conditions results in a positive precipitation anomaly (Fig. S23b) and a negative temperature anomaly (Fig. S23a), which together mitigate the adverse effects of high-temperature stress and water scarcity on maize production in NEC, thereby reducing CHDEs.

3.3. Comparison of two prediction models for maize production in NEC

Based on the above results, two prediction models for maize production in NEC are constructed in this section. Prediction Model #1 first establishes a prediction model for predicting DPI through stepwise regression of the four factors: SICI, SSTPI, SWI, and NAOI. The predicted DPI is then utilized as a predictor for DMAIZE. Prediction Model #2, on the other hand, directly predicts DMAIZE through stepwise regression of the four factors: SICI, SSTMI, SWI, and NAOI (Fig. 8).

3.3.1. Prediction model #1 and its performance

In Prediction Model #1, the correlation coefficients between the predictors (SICI, SSTPI, SWI, and NAOI) and DPI are –0.50, –0.28, 0.54 and –0.31, respectively, all of which are statistically significant at the 90 % confidence level based on the Student's *t*-test. Stepwise regression analysis identifies three independent factors—SICI, SSTPI and SWI—as predictors for the model, represented as follows:

$$DPI = -0.543 \times SICI - 0.347 \times SSTPI + 0.391 \times SWI + 0.013 \quad (3)$$

The partial correlation analysis indicate that SICI, SSTPI, and SWI independently influence DPI, with no multicollinearity issues (Tab. S1). The contribution rates of SICI, SSTPI, and SWI to DPI are 52.06 %, 21.10 %, and 26.85 %, respectively, with all of these values passing the Student's *t*-test at a 95 % confidence level (Tab. S2). The results indicate that the SICI is the most significant factor influencing DPI, followed by

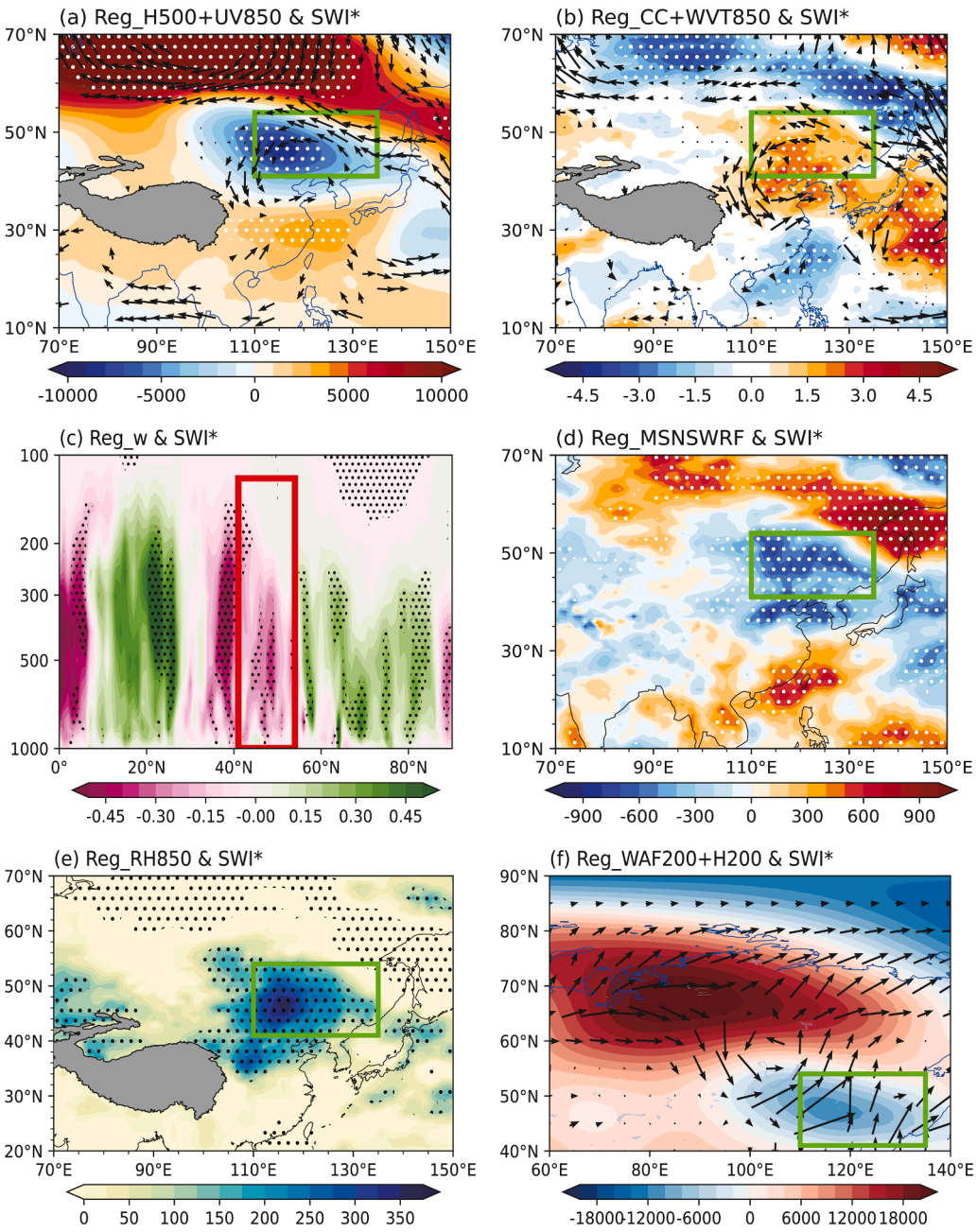

Fig. 5. Regression maps of the anomalous atmospheric circulations in summer with regard to SWI* [$SWI^* = SWI \times (-1)$]during 1980–2020: (a) 500 hPa geopotential height (shading) & 850 hPa wind (arrow), (b) fraction of cloud cover (shading) & 850 hPa water vapor transport (arrow), (c) vertical velocity averaged along 110°E–135°E vertical-latitudinal cross section, (d) surface net short wave radiation flux, (e) 850 hPa relative humidity, (f) 200 hPa wave flux (arrow) & geopotential height (shading). The regression coefficients within the dotted areas are significant at the 90 % confidence level based on the Student's *t*-test. The green rectangles denote NEC, whereas the red rectangle signifies the airspace over NEC.

SWI and SSTPI. The correlation coefficient between the observed and predicted values of DPI is 0.68, significant at the 99 % confidence level based on the Student's *t*-test. The predicted PI values are obtained by adding the predicted DPI values to the observed PI values from the preceding year, yielding a correlation coefficient of 0.61 (significant at the 99 % level based on the Student's *t*-test). The predicted DPI value further serves as an input for predicting DMAIZE using linear regression, modeled as follows:

$$DMAIZE = -0.466 \times DPI + 0.084 \quad (4)$$

In Prediction Model #1, the observed and predicted DMAIZE exhibit a strong correlation coefficient of 0.66 (significant at the 99 % confidence level based on the Student's *t*-test) (Fig. 8a). The predicted maize production from this model is computed by adding the predicted DMAIZE values to the observed maize production of the previous year, yielding a correlation coefficient of 0.90 between the observed and predicted maize production in NEC, also significant at the 99 % confidence level (Fig. 8c).

To further evaluate the efficacy of Prediction Model #1, independent hindcast tests and leave-one-out cross-validation tests are performed in this study. Both validation methods demonstrate satisfactory covariance between predicted and observed values. Specifically, in the independent hindcast tests, the correlation coefficient between the observed and predicted DPI values during 1996–2020 is 0.71 (Fig. S24a), while for PI, it is 0.51 (Fig. S24b). The correlation coefficient for predicted DMAIZE values is 0.64 (Fig. S24c), and for maize production values, it reaches

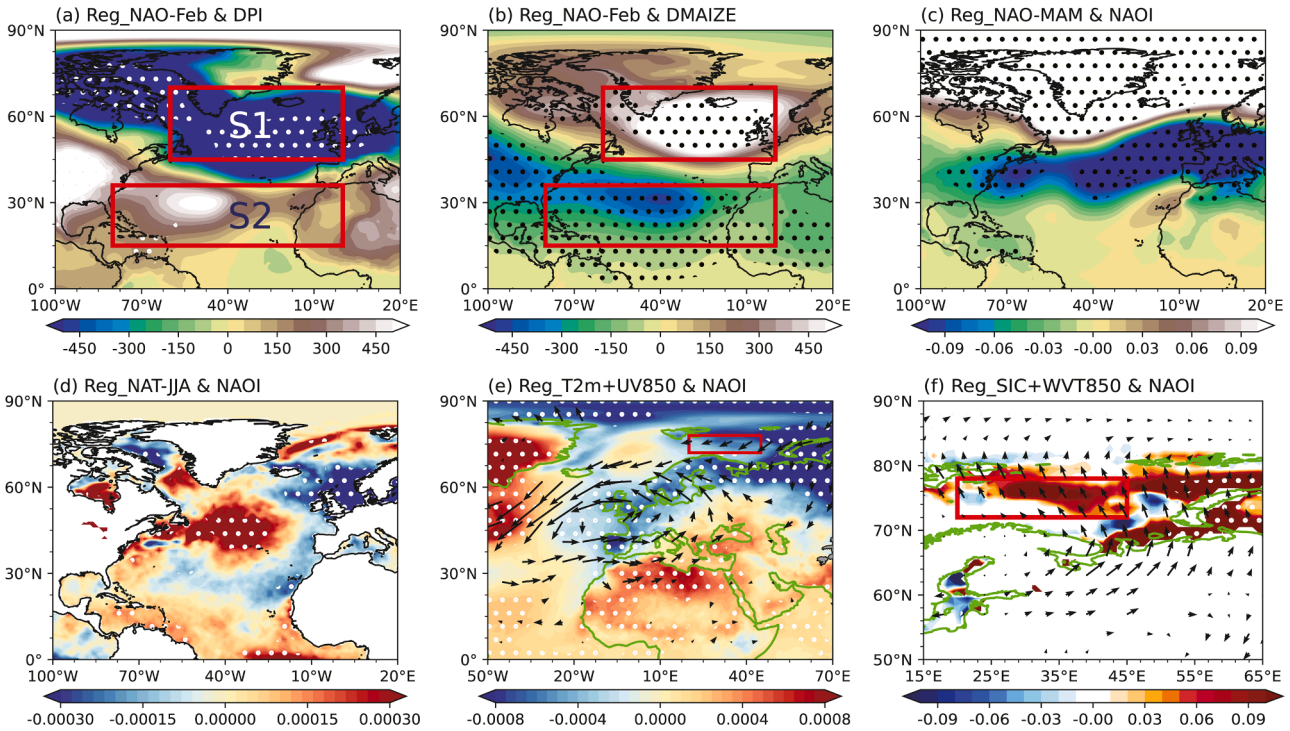

Fig. 6. Regression maps of sea level pressure in February with regard to (a) DPI, (b) DMAIZE. Regression maps of (c) sea level pressure in spring with regard to NAOI and the anomalous atmospheric circulations with regard to NAOI during 1980–2020: (d) SST in summer, (e) surface 2-m air temperature (shading) & 850 hPa wind (arrow) in spring, (f) sea ice concentration (shading) & 850 hPa water vapor transport (arrow) in spring. The regression coefficients within the dotted areas are significant at the 90 % confidence level based on the Student's *t*-test. The red rectangles in Fig. 6a and 6b denote the sea level pressure key regions for this study, where the results of the regional mean of sea level pressure in S1 minus sea level pressure in S2 in February is defined as NAOI. The red rectangles in Fig. 6e and 6f signify the sea ice concentration key regions, where the regional mean of sea ice concentration in May is defined as SICI.

0.72 (Fig. S24d). Similarly, the leave-one-out cross-validation tests yield correlation coefficients of 0.60, 0.56, 0.66, and 0.90 for predicted DPI, PI, DMAIZE, and maize production during 1980–2020, respectively (Fig. S25). All correlations mentioned are significant at the 99 % confidence level based on the Student's *t*-test. Therefore, Prediction Model #1 effectively captures the interannual variability of maize production in NEC.

3.3.2. Prediction model #2 and its performance

In Prediction Model #2, the predictors SICI, SSTMI, SWI, and NAOI, which are directly related to maize production in NEC, are utilized for stepwise regression. The correlation coefficients for these factors with DMAIZE are 0.33, 0.46, –0.65, and 0.44, demonstrating significance at the 95 %, 99 %, 99 %, and 99 % confidence levels, respectively. Ultimately, the predictive equation for DMAIZE in Prediction Model #2, based on two selected independent factors (SSTMI and SWI), is formulated as follows:

$$DMAIZE = 0.203 \times SSTMI - 0.349 \times SWI + 0.078 \quad (5)$$

The partial correlation analysis indicate that SSTMI and SWI independently influence DMAIZE, with no multicollinearity issues (Tab. S3). The contribution rates of SSTMI and SWI in the prediction model are 25.26 % and 74.74 %, respectively, highlighting that SWI is the most significant factor influencing DMAIZE in Prediction Model #2 (Tab. S4). The results indicate a strong correlation coefficient of 0.73 between the observed and predicted DMAIZE from Prediction Model #2, which is significant at the 99 % confidence level based on the Student's *t*-test (Fig. 8b). The maize production predicted by this model is derived by adding the predicted DMAIZE to the observed maize production from the previous year, resulting in a correlation coefficient of 0.91 with the observed maize production, also significant at the 99 % confidence level (Fig. 8d).

Furthermore, the independent hindcast tests show a correlation coefficient of 0.75 between the observed and predicted DMAIZE during 1996–2020 (Fig. S26a), while the correlation coefficient between the observed and predicted maize production is 0.79 (Fig. S26b). Similarly, the leave-one-out cross-validation tests for Prediction Model #2 show a DMAIZE predicting effect of 0.68 and a maize production effect of 0.90 during 1980–2020 (Fig. S27). All correlations discussed above have successfully passed the Student's *t*-test for confidence at the 99 % level, indicating that Prediction Model #2 effectively captures and accurately predicts annual maize production in NEC.

3.3.3. Comparison and evaluation of the two prediction models

Both prediction models proposed in this study demonstrate robust performance in predicting maize production in NEC. However, subtle differences exist between the models, particularly in terms of prediction period validity and overall performance.

$$DMAIZE = \begin{cases} -0.466 \times DPI + 0.084, & PM1 \\ 0.203 \times SSTMI - 0.349 \times SWI + 0.078, & PM2 \end{cases} \quad (6)$$

Prediction Model #1 incorporates three predictors (SICI, SSTPI, and SWI) associated with the months of May, February, and April, respectively, allowing predictions for CHDEs and maize production at the end of May. In contrast, Prediction Model #2 utilizes two predictors (SSTMI and SWI) based on data from February and April, enabling predictions by the end of April. Given that maize in NEC matures between late September and early October, Prediction Model #1 has a prediction period validity of four months, while Prediction Model #2 extends this to five months. In terms of prediction performance, Prediction Model #1 is capable for predicting summer CHDEs in NEC, whereas Prediction Model #2 is not. Despite both prediction models have passed the significance test at the 99 % level, Prediction Model #1 exhibits a slightly lower prediction performance for DMAIZE compared to Prediction

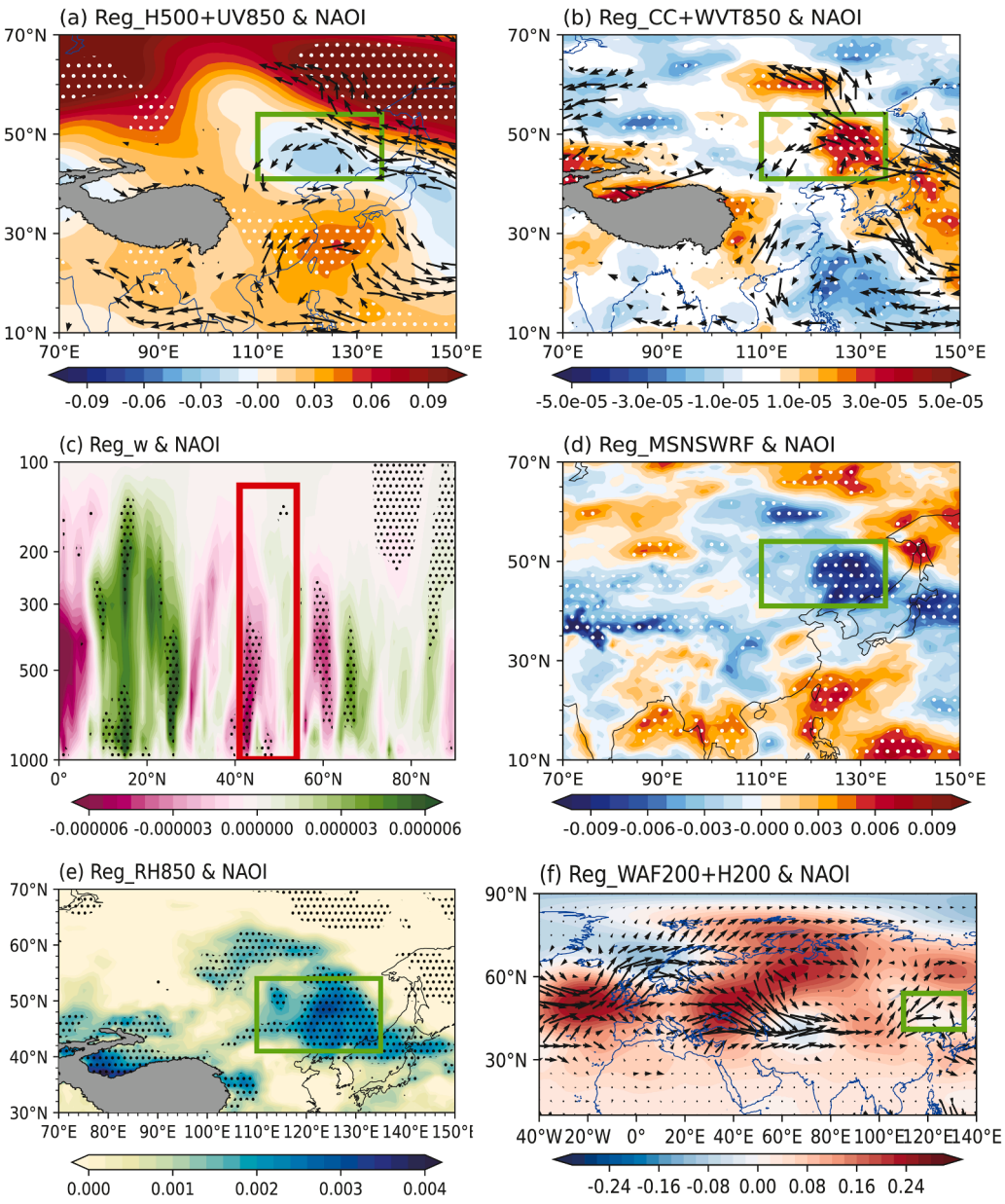

Fig. 7. Regression maps of the anomalous atmospheric circulations in summer with regard to NAOI during 1980–2020: (a) 500 hPa geopotential height (shading) & 850 hPa wind (arrow), (b) fraction of cloud cover (shading) & 850 hPa water vapor transport (arrow), (c) vertical velocity averaged along 110°E–135°E vertical-latitudinal cross section, (d) surface net short wave radiation flux, (e) 850 hPa relative humidity, (f) 200 hPa wave flux (arrow) & geopotential height (shading). The regression coefficients within the dotted areas are significant at the 90 % confidence level based on the Student's *t*-test. The green rectangles denote NEC, whereas the red rectangle signifies the airspace over NEC.

Model #2.

When compared to previous maize production prediction models in NEC proposed by Zhou et al. (2017), the models developed in this study demonstrate significantly improved robustness. Zhou et al. (2017) reported a correlation coefficient of 0.538 for observed and predicted year-to-year increment maize production during 1969–2008 (40 years), whereas the Prediction Model #1 and Prediction Model #2 in this study yield correlation coefficients of 0.66 and 0.73 during 1980–2020 (41 years), respectively.

Additionally, as the models developed in this study are based on CHDEs during summer, they are particularly adept at predicting extreme variability in maize production in NEC. We computed the absolute values of the observed DMAIZE and identified the top twenty years with the highest absolute DMAIZE, as well as the remaining twenty-one years out of the total 41 years. For these two subsets of years, we calculated correlation coefficients between observed and predicted DMAIZE. The results indicate that Prediction Model #1 achieves a prediction performance of 0.74 for the top twenty years with the highest absolute DMAIZE, passing the Student's *t*-test at a 99 % confidence level (Fig. S28a), while the performance drops to 0.45 for the remaining twenty-one years (Fig. S28b). Similarly, Prediction Model #2 yields a correlation coefficient of 0.78 for the top twenty years (Fig. S29a) and 0.56 for the remaining years (Fig. S29b). Therefore, the maize production prediction models developed in this study are more effective in predicting extreme events while demonstrating reduced efficacy in years with minimal variability. It is noteworthy that larger interannual variations in maize production yield greater impact and research significance, whereas smaller variations possess diminished forecasting need.

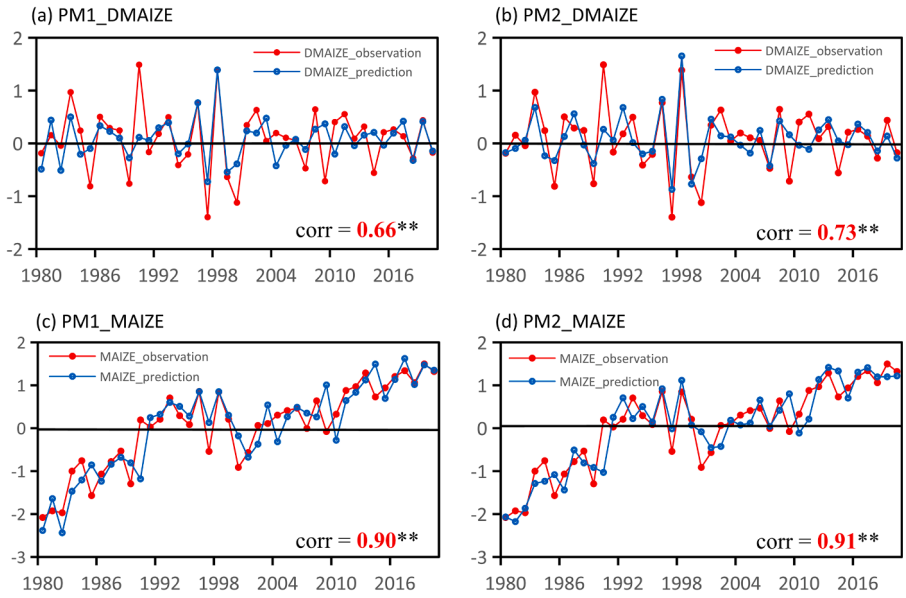

Fig. 8. Temporal series of (a) DMAIZE, (c) maize production observation (red line) with prediction (blue line) values during 1980–2020 in Prediction Model #1. Temporal series of (b) DMAIZE, (d) maize production observation (red line) with prediction (blue line) values during 1980–2020 in Prediction Model #2. Based on the Student's *t*-test, the correlation coefficients significant at the 99 % confidence level are indicated by two asterisks.

4. Conclusion and discussion

This study investigates the underlying physical mechanism of CHDEs and their impacts on maize production, while also developing two prediction models for maize production. The results reveal that the CHDEs in NEC are associated with high temperature stress and the water scarcity, resulting in reduced maize production. Additionally, significant correlations are observed between sea ice concentration in the Barents Sea, El Niño-like SST in the equatorial East Pacific, soil water in northwestern Siberia, and the NAO in North Atlantic with CHDEs and maize production in NEC.

Fig. 9 illustrates the physical mechanisms through which these factors influence NEC. Notably, increased sea ice concentration in the Barents Sea during May can persist into summer, driven by the continuity of sea ice and contributions from Siberian snow. This phenomenon enhances the POL-like wave train in summer (IV), leading to atmospheric circulation anomalies that subsequently affect maize production in NEC. Additionally, warm SST anomalies in the equatorial East Pacific during the preceding winter facilitate the transport and retention of these warm SST signals via the Indian Ocean's "capacitor" effect, enhancing the Western North Pacific Anomalous Anticyclone through eastward-propagating equatorial Kelvin waves and reinforcing

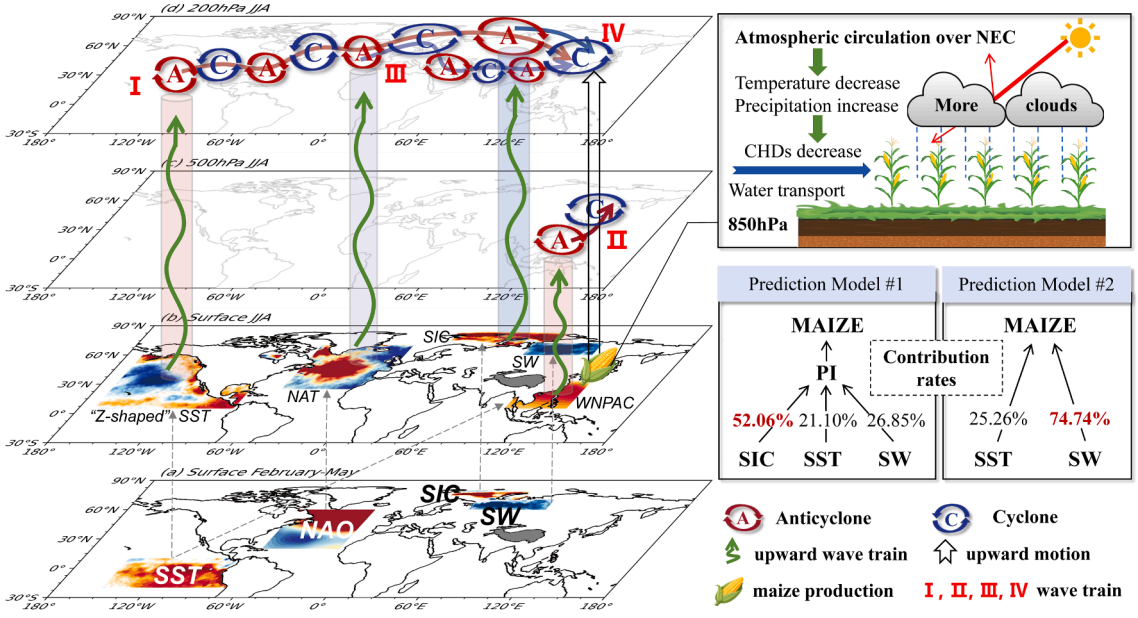

Fig. 9. A map summarizing the physical mechanisms by which sea ice concentration (SIC), sea surface temperature (SST), soil water (SW) and North Atlantic Oscillation (NAO) influence atmospheric circulation conditions, CHDEs and maize production in NEC. The diagram in the upper right depicts the physical mechanisms by which atmospheric circulation influences CHDEs. The Prediction Model #1 utilizes three factors—SIC, SST, SW—to predict the PI. Subsequently, the predicted PI values are employed to predict MAIZE. Prediction Model #2 directly employs SST and SW to predict MAIZE. The percentages displayed above the models represent the relative contributions of each factor to the prediction target, with the red percentages indicating the dominant influencing factors.

northward propagating Pacific-Japan teleconnection wave trains at 500 hPa (II) in summer. Concurrently, winter warm SST anomalies in the equatorial East Pacific can induce "Z-shaped" SST anomalies in the North Pacific via poleward Kelvin waves in summer, which enhances atmospheric disturbances and stimulates an upward wave train that infiltrates the subtropical westerly jet stream at 200 hPa, subsequently propagating eastward from the west coast of North America to NEC (I). Furthermore, the negative soil water anomalies in northwestern Siberia in April influence NEC in summer by affecting evaporation processes in Siberia, thereby enhancing the wave train directed to NEC (IV). Moreover, the February NAO maintains its influence into summer via the NAT, initiating an eastward propagating Rossby wave train at 200 hPa (III) via robust air-sea interactions. Notably, the February NAO also affects atmospheric processes that lead to increased spring sea ice in the Barents Sea, which functions as a "capacitor" further modulating atmospheric circulation in NEC during summer.

Based on these physical mechanisms, this study constructs two prediction models employing a year-to-year increment method. In Prediction Model #1, four predictors—SICI, SSTPI, SWI and NAOI—are initially considered for stepwise regression analysis. Ultimately, SICI, SSTPI, and SWI are incorporated into the predictive equation for DPI, which is subsequently used to predict DMAIZE in NEC. In Prediction Model #2, stepwise regression identifies SSTMI and SWI from the predictors SICI, SSTMI, SWI, and NAOI to directly predict maize production in NEC. The results demonstrate that both prediction models accurately predict DMAIZE, as validated through leave-one-out cross-validation tests and independent hindcast tests. Furthermore, these models exhibit superior predictive performance for extreme interannual incremental values in maize production, underscoring their practical significance.

Of particular note, the CHDEs that occurred in NEC in 2018 had a substantial impact on crops, with both Prediction Model #1 and #2 accurately capturing the decline in maize production. Specifically, the observed DMAIZE for 2018 was –0.28, with a corresponding maize production of 1.06. Prediction Model #1 predicts a DMAIZE of –0.32 and a maize production of 1.02 in 2018, demonstrating a satisfactory predictive capability. In Prediction Model #2, the 2018 DMAIZE prediction is –0.14, while the maize production prediction is 1.20. Thus, both prediction successfully forecasted CHDEs in NEC four to five months in advance in 2018, which is crucial for effective crop management.

In this study, we investigate the physical mechanisms by which large-scale climate factors influence CHDEs and maize production in NEC. These factors, including sea ice concentration, SST, soil water, and NAO, modulate atmospheric circulation patterns over the NEC during summer, thereby affecting local temperature and precipitation conditions. These conditions are critical in shaping CHDEs and maize production. While local temperature and precipitation are key factors, we also explored their direct utility in predicting maize production in NEC. Monthly correlations between temperature, precipitation, and maize production from March to August are analyzed, revealing the strongest relationships between maize production and July precipitation and August temperature, both of which pass the Student's *t*-test at a 99 % confidence level (Fig. S30). Although the model incorporating these two variables achieve a high correlation coefficient of 0.87 (significant at the 99 % confidence level based on a Student's *t*-test) (Fig. S31), its predictive performance is still inferior to that of the model based on large-scale meteorological factors, which achieve a correlation coefficient of 0.91 (Fig. 8). Additionally, predictions based solely on local temperature and precipitation can only be issued by late August (Fig. S30), limiting their prediction period validity.

In contrast, the model constructed using large-scale climate factors provides a more comprehensive representation of the local meteorological conditions influencing maize. These local conditions are complex and interdependent, encompassing more than just temperature and precipitation. Predicting maize production based solely on some local meteorological variables may overlook critical factors. Furthermore, large-scale factors change more slowly and are more stable and reliable for prediction compared to rapidly changing local weather variables.

Lesk et al. (2021) demonstrated that both atmospheric circulation and temperature-moisture couplings exacerbate CHDEs risks, with moisture playing a critical role in modulating these events. Temperature-moisture couplings reduce soil moisture through extreme heat, decrease evapotranspiration, enhance sensible heat flux, creating positive feedback that intensifies CHDEs (Lesk et al., 2021; Seo et al., 2022; Ni et al., 2024). While this study primarily focuses on the long-term CHDEs and maize production prediction in NEC, with particular emphasis on the role of precursor factors in atmospheric circulation mechanisms as effective predictors, we prioritize the examination of atmospheric circulation mechanisms. Nonetheless, it is important to note that local soil moisture anomalies (Fig. S32c) and temperature-moisture couplings (Fig. S32d) may also exacerbate CHDEs in NEC through positive feedback mechanisms (Seo et al., 2022; Ni et al., 2024), posing significant threats to maize production in the region (Fig. S32a and S32b).

Additionally, this study focuses specifically on the physical mechanisms by which Barents Sea ice, equatorial East Pacific sea surface temperature, northwest Siberian soil water, and NAO influence CHDEs in NEC through some defined pathways. However, the factors discussed may also exert influence through alternative routes. Previous researchers have identified additional variables, such as Bering Sea ice (Zhou and Wang., 2014; Tian et al., 2021), Nansen Basin Sea ice (Lin et al., 2023), and Indian Ocean Dipole SST (Lin et al., 2023), which may also impact temperature and precipitation patterns in NEC through the Urals High (Lin et al., 2023) and the Subtropical High (Liu et al., 2015; Wang et al., 2015; Du et al., 2021). Consequently, further researches are warranted to attain a more comprehensive understanding of the mechanisms underlying CHDEs in this region.

CRediT authorship contribution statement

Yeran Zhou: Writing – original draft, Software, Investigation, Formal analysis. **Huixin Li:** Writing – review & editing, Methodology, Investigation, Data curation, Conceptualization. **Bo Sun:** Writing – review & editing, Investigation, Conceptualization. **Huijun Wang:** Writing – review & editing, Supervision, Conceptualization. **Hui Ju:** Writing – review & editing. **Yuan Yuan:** Writing – review & editing. **Jiani Zeng:** Writing – review & editing.

Declaration of competing interest

The authors declare that they have no known competing financial interests or personal relationships that could have appeared to influence the work reported in this paper.

Acknowledgments

This work was supported by the National Natural Science Foundation of China [grant number 42088101]; and the National Undergraduate Innovation and Entrepreneurship Training Program [grant number 202410300001Z].

Supplementary materials

Supplementary material associated with this article can be found, in the online version, at doi:10.1016/j.agrformet.2025.110709.

Data availability

Data will be made available on request.

References

Aroca, R., Irigoyen, J.J., Sánchez-Díaz, M., 2003. Drought enhances maize chilling tolerance. II. Photosynthetic traits and protective mechanisms against oxidative stress. Physiol. Plant. 117 (4), 540–549.

Bai, L.P., Sui, F.G., Ge, T.D., Sun, Z.H., Lu, Y.Y., Zhou, G.S., 2006. Effect of soil drought stress on leaf water status, membrane permeability and enzymatic antioxidant system of maize. Pedosphere 16 (3), 326–332.

Bishop, C.M., 2006. Pattern Recognition and Machine Learning. Springer, New York.

Bring, J., 1994. How to standardize regression coefficients. Am. Stat. 48 (3), 209–213.

Campos, H., Cooper, M., Habben, J.E., Edmeades, G.O., Schussler, J.R., 2004. Improving drought tolerance in maize: a view from industry. Field. Crops. Res. 90 (1), 19–34.

Carnes, B.A., Slade, N.A., 1988. The use of regression for detecting competition with multicollinear data. Ecology 69 (4), 1266–1274.

Chatterjee, S., Desai, A.R., Zhu, J., Townsend, P.A., Huang, J.Y., 2022. Soil moisture as an essential component for delineating and forecasting agricultural rather than meteorological drought. Remote. Sens. Env. 269, 112833.

Chelton, D.B., Davis, R.E., 1982. Monthly mean sea-level variability along the west coast of North America. J. Phys. Oceanogr. 12, 757–784.

Chen, D., Gao, Y., Zhang, Y., Wang, T., 2022. Effects of spring Arctic sea ice on summer drought in the middle and high latitudes of Asia. Atmos. Ocean. Sci. Lett. 15 (3), 100138.

Chen, D., Sun, Q.Z., 2024. Impact of rapid Arctic sea ice decline on China's crop yield under global warming. Environ. Dev. Sustain. 26 (1), 1263–1280.

Chen, H.P., Sun, J.Q., 2015. Changes in drought characteristics over China using the standardized precipitation evapotranspiration index. J. Clim. 28 (13), 5430–5447.

Chen, Z.S., Wen, Z.P., Wu, R.G., Du, Y., 2017. Roles of tropical SST anomalies in modulating the western north Pacific anomalous cyclone during strong La Nia decaying years. Clim. Dyn. 49 (1–2), 633–647.

Cohen, J., Cohen, P., West, S.G., Aiken, L.S., 2003. Applied Multiple Regression/ Correlation Analysis for the Behavioral Sciences, 3rd ed. Routledge, New York.

Cui, Y.F., Duan, A.M., Liu, Y.M., Wu, G.X., 2015. Interannual variability of the spring atmospheric heat source over the Tibetan Plateau forced by the North Atlantic SSTA. Clim. Dyn. 45 (5–6), 1617–1634.

Dai, H.X., Fan, K., 2021. An effective downscaling model for operational prediction of summer precipitation over China. Atmos. Res. 257, 105621.

Darlington, R.B., Hayes, A.F., 2017. Regression Analysis and Linear Models: Concepts, Applications, and Implementation. The Guilford Press, New York.

Du, Y.B., Zhang, J., Zhao, S.W., Chen, Z.H., 2021. A mechanism of spring Barents Sea ice effect on the extreme summer droughts in northeastern China. Clim. Dyn. 58 (3–4), 1033–1048.

Du, Y.C., Chen, H.P., 2025. Synergistic influence of Eurasian soil moisture and Pacific sea surface temperature anomalies on August out-of-phase precipitation pattern in northern China. J. Geophys. Res. Atmos. 130 (5), e2024JD042888.

Erenstein, O., Jaleta, M., Sonder, K., Mottaleb, K., Prasanna, B.M., 2022. Global maize production, consumption and trade: trends and R&D implications. Food Sec. 14, 1295–1319.

Fan, K., 2010. A prediction model for Atlantic named storm frequency using a year-by-year increment approach. Wea. fcst. 25 (6), 1842–1851.

Fan, K., Wang, H.J., Choi, Y.J., 2008. A physically-based statistical forecast model for the middle-lower reaches of the Yangtze River Valley summer rainfall. Chin. Sci. Bull. 53 (4), 602–609.

Feng, J., Chen, W., 2021. Roles of the North Indian Ocean SST and tropical North Atlantic SST in the latitudinal extension of the anomalous western North Pacific anticyclone during the El nio decaying summer. J. Clim. 34 (21), 8503–8517.

Feng, J., Chen, W., 2022. Respective and combined impacts of North Indian Ocean and tropical North Atlantic SST anomalies on the subseasonal evolution of anomalous western North Pacific anticyclones. J. Clim. 35 (17), 5623–5636.

Gao, Y.Q., Sun, J.Q., Li, F., He, S.P., Sandven, S., Yan, Q., Zhang, Z.S., Lohmann, K., Keenlyside, N., Furevik, T., Suo, L.L., 2015. Arctic sea ice and Eurasian climate: a review. Adv. Atmos. Sci. 32 (1), 92–144.

Ha, T.T.V., Fan, H.L., Shuang, L., 2021. Climate change impact assessment on Northeast China's grain production. Environ. Sci. Pollut. Res. 28 (12), 14508–14520.

Hao, S.B., Li, J.D., Mao, J.Y., 2022. Interannual relationship between summer North Atlantic Oscillation and subsequent November precipitation anomalies over Yunnan in southwest China. J. Meteorol. Res. 36 (5), 718–732.

Haro-Monteagudo, D., Solera, A., Andreu, J., 2017. Drought early warning based on optimal risk forecasts in regulated river systems: application to the Jucar River Basin (Spain). J. Hydrol. 544, 36–45.

He, S.P., Gao, Y.Q., Furevik, T., Wang, H.J., Li, F., 2018. Teleconnection between sea ice in the Barents Sea in June and the Silk Road, Pacific–Japan and East Asian rainfall patterns in August. Adv. Atmos. Sci. 35 (1), 52–64.

Inoue, J., Hori, M.E., Takaya, K., 2012. The Role of Barents Sea Ice in the Wintertime Cyclone Track and Emergence of a Warm-Arctic Cold-Siberian Anomaly. J. Clim. 25, 2561–2568.

Jiang, J.L., Liu, Y.M., Mao, J.Y., Wu, G.X., 2023. Extreme heatwave over Eastern China in summer 2022: the role of three oceans and local soil moisture feedback. Environ. Res. Lett. 18 (4), 044025.

Ju, H., van der Velde, M., Lin, E.D., Xiong, W., Li, Y.C., 2013. The impacts of climate change on agricultural production systems in China. Clim. Change 120 (1–2), 313–324.

Kent, C., Pope, E., Dunstone, N., Scaife, A.A., Tian, Z., Clark, R., Zhang, L., Davie, J., Lewis, K., 2019. Maize drought hazard in the Northeast farming region of China: unprecedented events in the current climate. J. Appl. Meteorol. Climatol. 58 (10), 2247–2258.

Kim, K.H., Lee, B.M., 2023. Effects of climate change and drought tolerance on maize growth. Plants 12 (20), 3548.

Kim, B.M., Son, S.W., Min, S.K., et al., 2014. Weakening of the stratospheric polar vortex by Arctic sea-ice loss. Nat. Commun. 5, 4646.

Lesk, C., Coffel, E., Winter, J., Ray, D., Zscheischler, J., Seneviratne, S.I., Horton, R., 2021. Stronger temperature–moisture couplings exacerbate the impact of climate warming on global crop yields. Nat. Food 2, 683–691.

Lesk, C., Rowhani, P., Ramankutty, N., 2016. Influence of extreme weather disasters on global crop production. Nature 529, 84–87.

Li, E., Zhao, J., Zhang, W.M., Yang, X.G., 2023. Spatial-temporal patterns of high-temperature and drought during the maize growing season under current and future climate changes in northeast China. J. Sci. Food Agric. 103 (12), 5709–5716.

Li, H.X., Chen, H.P., Wang, H.J., Sun, J.Q., Ma, J.H., 2018. Can Barents Sea ice decline in spring enhance summer hot drought events over northeastern China? J. Clim. 31 (12), 4705–4725.

Li, H.X., He, S.P., Gao, Y.Q., Chen, H.P., Wang, H.J., 2020. North Atlantic modulation of interdecadal variations in hot drought events over northeastern China. J. Clim. 33 (10), 4315–4332.

Li, H.X., Sun, B., Wang, H.J., Zhou, B.T., Duan, M.K., 2022a. Mechanisms and physical-empirical prediction model of concurrent heatwaves and droughts in July-August over northeastern China. J. Hydrol. 614, 128535.

Li, H.X., Sun, B., Zhang, Z.S., Wang, H.J., Zhou, Y.R., Zeng, J.N., Zhou, B.T., 2025. Compound hot drought events in the Mei-yu region: influences from polar and tropical regions. Sci. Bull. 70 (2), 273–282.

Li, T., Zhang, X.P., Liu, Q., Liu, J., Chen, Y.Q., Sui, P., 2022b. Yield penalty of maize (Zea mays L.) under heat stress in different growth stages: a review. J. Integr. Agric. 21 (9), 2465–2476.

Lin, Y.T., Fang, Y.H., Zhao, C.Y., Gong, Z.Q., Yang, S.Q., Yu, Y.Q., 2023. The coordinated influence of Indian Ocean sea surface temperature and Arctic Sea ice on anomalous Northeast China cold vortex activities with different paths during late summer. Adv. Atmos. Sci. 40 (1), 62–77.

Lin, Z.D., Li, F., 2018. Impact of interannual variations of spring sea ice in the Barents Sea on East Asian rainfall in June. Atmos. Oceanic. Sci. Lett. 11 (3), 275–281.

Liu, G., Feng, G.L., Qin, Y.L., Cao, L., Yao, H.W., Liu, Z.Q., 2015. Activity of cold vortex in northeastern China and its connection with the characteristics of precipitation and circulation during 1960–2012. J. Geogr. Sci. 25 (12), 1423–1438.

Liu, X.W., Wang, X.L., Wang, X.Y., Gao, J., Luo, N., Meng, Q.F., Wang, P., 2020. Dissecting the critical stage in the response of maize kernel set to individual and combined drought and heat stress around flowering. Env. Exp. Bot. 179, 104213.

Liu, X.W., Yu, Y.H., Huang, S.B., Xu, C.C., Wang, X.Y., Gao, J., Meng, Q.F., Wang, P., 2022. The impact of drought and heat stress at flowering on maize kernel filling: insights from the field and laboratory. Agric. Meteorol. 312, 108733.

Ma, X.W., Su, Z., Ma, H., 2020. Molecular genetic analyses of abiotic stress responses during plant reproductive development. J. Exp. Bot. 71 (10), 2870–2885.

Menard, S., 2004. Standardized regression coefficients. In: Lewis-Beck, M.S., Bryman, A., Liao, T.F. (Eds.), The Sage Encyclopedia of Social Science Research Methods. Sage Publications, California, pp. 1069–1070.

Ni, Y.Y., Qiu, B., Miao, X., Li, L.F., Chen, J.Y., Tian, X.H., Zhao, S.W., Guo, W.D., 2024. Shift of soil moisture-temperature coupling exacerbated 2022 compound hot-dry event in eastern China. Environ. Res. Lett. 19, 014059.

Nielsen, D.C., Vigil, M.F., Benjamin, J.G., 2009. The variable response of dryland corn yield to soil water content at planting. Agric. Water. Manag. 96 (2), 330–336.

Petoukhov, V., Semenov, V.A., 2010. A link between reduced Barents-Kara sea ice and cold winter extremes over northern continents. J. Geophys. Res. 115, D21111.

Ray, D.K., Gerber, J.S., MacDonald, G.K., West, P.C., 2015. Climate variation explains a third of global crop yield variability. Nat. Commun. 6, 5989.

Sang, Y., Ren, H.L., Deng, Y., Xu, X.F., Shi, X.L., Zhao, S., 2022. Impacts of late-spring north eurasian soil moisture variation on summer rainfall anomalies in Northern East Asia. Clim. Dyn. 58 (5–6), 1495–1508.

Seo, Y.W., Ha, K.J., 2022. Changes in land-atmosphere coupling increase compound drought and heatwaves over northern East Asia. npj Clim. Atmos. Sci. 5, 100.

Song, Y.L., Linderholm, H.W., Luo, Y., Xu, J.X., Zhou, G.S., 2020. Climatic causes of maize production loss under global warming in Northeast China. Sustainability 12 (18), 7829.

Song, Y.L., Tian, J.F., Linderholm, H.W., Wang, C.Y., Ou, Z.R., Chen, D.L., 2021. The contributions of climate change and production area expansion to drought risk for maize in China over the last four decades. Int. J. Climatol. 41, E2851–E2862.

Sun, Y., Chen, H.S., Zhu, S.G., Zhang, J., Wei, J.F., 2021. Influence of the Eurasian spring snowmelt on summer land surface warming over Northeast Asia and its associated mechanism. J. Clim. 34 (12), 4851–4869.

Tao, F.L., Zhang, Z., Zhang, S., Zhu, Z., Shi, W.J., 2012. Response of crop yields to climate trends since 1980 in China. Clim. Res. 54, 233–247.

Tao, Z.Q., Chen, Y.Q., Li, C., Zou, J.X., Yan, P., Yuan, S.F., Wu, X., Sui, P., 2016. The causes and impacts for heat stress in spring maize during grain filling in the North China Plain - A review. J. Integr. Agric. 15 (12), 2677–2687.

Tian, Y.R., Gao, Y.Q., Guo, D., 2021. The relationship between melt season sea ice over the Bering Sea and summer precipitation over Mid-Latitude East Asia. Adv. Atmos. Sci. 38 (6), 918–930.

Tonidandel, S., LeBreton, J.M., 2021. Relative importance analysis: a useful supplement to regression analysis. J. Bus. Psychol. 26, 1–9.

Venkatappa, M., Sasaki, N., Han, P., Abe, I., 2021. Impacts of droughts and floods on croplands and crop production in Southeast Asia-an application of Google Earth Engine. Sci. Total Environ. 795, 148829.

Wang, C.Y., Linderholm, H.W., Song, Y.L., Wang, F., Liu, Y.J., Tian, J.F., Xu, J.X., Song, Y.B., Ren, G.Y., 2020. Impacts of drought on maize and soybean production in Northeast China during the past five decades. IJERPH. 17 (7), 2459.

Wang, H.J., He, S.P., 2015. The North China/northeastern Asia severe summer drought in 2014. J. Clim. 28 (17), 6667–6681.
Wang, S.S., Yuan, X., Wu, R.G., 2019a. Attribution of the persistent spring-summer hot and dry extremes over Northeast China in 2017. Bull. Am. Meteorol. Soc. 100 (1), S85–S89.
Wang, Y.Y., Tao, H.B., Tian, B.J., Sheng, D.C., Xu, C.C., Zhou, H.M., Huang, S.B., Wang, P., 2019b. Flowering dynamics, pollen, and pistil contribution to grain yield in response to high temperature during maize flowering. Env. Exp. Bot. 158, 80–88.
Webber, H., Ewert, F., Olesen, J.E., Müller, C., Fronzek, S., Ruane, A.C., Bourgault, M., Martre, P., Ababaei, B., Bindi, M., Ferrise, R., Finger, R., Fodor, N., Gabaldón-Leal, C., Gaiser, T., Jabloun, M., Kersebaum, K.C., Lizaso, J.I., Lorite, I.J., Manceau, L., Moriondo, M., Nendel, C., Rodríguez, A., Ruiz-Ramos, M., Semenov, M. A., Siebert, S., Stella, T., Stratonovitch, P., Trombi, G., Wallach, D., 2018. Diverging importance of drought stress for maize and winter wheat in Europe. Nat. Commun. 9, 4249.
Wen, N., Laurent, L., Hao, Y.S., 2022. Response of East Asian summer precipitation to intermediate SST anomalies while El Niño decays and dependence on type of events. J. Clim. 35 (12), 3845–3860.
Wu, B., Zhou, T.J., Li, T., 2009. Seasonally evolving dominant interannual variability modes of East Asian climate. J. Clim. 22 (11), 2992–3005.
Wu, B., Li, T., Zhou, T.J., 2010. Relative contributions of the Indian Ocean and local SST anomalies to the maintenance of the western North Pacific anomalous anticyclone during the El Niño decaying summer. J. Clim. 23 (11), 2974–2986.
Wu, J., Gao, X.J., 2013. A gridded daily observation dataset over China region and comparison with the other datasets. Chin. J. Geophys. 56 (4), 1102–1111 in Chinese.
Wu, Y.X., Zhou, G.S., Song, Y.L., Zhou, L., 2024. Thresholds and extent of temperature effects on maize yield differ in different grain-filling stages. Sci. Total Environ. 918, 170709.
Xie, S.P., Hu, K.M., Hafner, J., Tokinaga, H., Du, Y., Huang, G., Sampe, T., 2009. Indian Ocean capacitor effect on Indo-Western Pacific climate during the summer following El Nino. J. Clim. 22 (3), 730–747.
You, L.Z., Rosegrant, M.W., Wood, S., Sun, D.S., 2009. Impact of growing season temperature on wheat productivity in China. Agric. Meteorol. 149 (6–7), 1009–1014.
Yu, X.F., Qu, J.W., Hu, S.P., Xu, P., Chen, Z.X., Gao, J.L., Ma, D.L., 2023. The effect of tillage methods on soil physical properties and maize yield in Eastern Inner Mongolia. Eur. J. Agron. 147, 126852.
Yule, G.U., 1907. On the theory of correlation for any number of variables, treated by a new system of notation. Proc. R. Soc. Lond. A 79 (529), 182–193.
Zeng, H.L., Xiao, C., Chen, X.Y., YE, D.X., 2019. State of China's climate in 2018. Atmos. Oceanic. Sci. Lett. 12 (5), 349–354.
Zhang, P., Wu, Z.W., Jin, R., 2021. How can the winter North Atlantic Oscillation influence the early summer precipitation in Northeast Asia: effect of the Arctic sea ice. Clim. Dyn. 56 (5–6), 1989–2005.
Zhang, Q., Hu, Z.H., 2018. Assessment of drought during maize growing season in Northeast China. Theor. Appl. Clim. 133 (3–4), 1315–1321.
Zhang, R., Zuo, Z., 2011. Impact of spring soil moisture on surface energy balance and summer monsoon circulation over East Asia and precipitation in east China. J. Clim. 24, 3309–3322.
Zhou, M.Z., Wang, H.J., 2014. Late winter sea ice in the Bering Sea: predictor for maize and rice production in Northeast China. J. Appl. Meteorol. Climatol. 53 (5), 1183–1192.
Zhou, M.Z., Wang, H.J., Huo, Z.G., 2017. A new prediction model for grain production in Northeast China based on spring North Atlantic Oscillation and late-winter Bering Sea ice cover. J. Meteorol. Res. 31 (2), 409–419.
Zhou, M.Z., Wang, H.J., Yang, S., Fan, K., 2013. Influence of springtime North Atlantic oscillation on crops productions in Northeast China. Clim. Dyn. 41 (11–12), 3317–3324.
Zhu, Z.W., Feng, Y.N., Jiang, W., Lu, R., Yang, Y., 2023. The compound impacts of sea surface temperature modes in the Indian and North Atlantic oceans on the extreme precipitation days in the Yangtze River Basin. Clim. Dyn. 61, 3327–3341.
Zomer, R.J., Xu, J., Trabucco, A., 2022. Version 3 of the global aridity index and potential evapotranspiration database. Sci. Data 9 (1), 409.